Rad51 filaments assembled in the absence of the complex formed by the Rad51 paralogs Rad55 and Rad57 are outcompeted by translesion DNA polymerases on UV-induced ssDNA gaps

Laurent Maloisel[1,*], Émilie Ma[1], Jamie Phipps[1], Alice Deshayes[1], Stefano Mattarocci[1], Stephane Marcand[1], Karine Dubrana[1] and Éric Coïc[1,*]

[1]Université de Paris and Université Paris-Saclay, INSERM, CEA, Institut de Biologie François Jacob, UMR Stabilité Génétique Cellules Souches et Radiations, F-92265 Fontenay-aux-Roses, France.

[*]Corresponding authors

E-mails: eric.coic@cea.fr; laurent.maloisel@cea.fr

Keywords: Rad51 paralogs, Rad55-Rad57, homologous recombination, translesion polymerases, Polζ, Polη.

Running title: Rad55-Rad57 prevents recruitment of translesion DNA polymerases

Abstract

The bypass of DNA lesions that block replicative polymerases during DNA replication relies on DNA damage tolerance pathways. The error-prone translesion synthesis (TLS) pathway depends on specialized DNA polymerases that incorporate nucleotides in front of base lesions, potentially inducing mutagenesis. Two error-free pathways can bypass the lesions: the template switching pathway, which uses the sister chromatid as a template, and the homologous recombination pathway (HR), which also can use the homologous chromosome as template. The balance between error-prone and error-free pathways controls the mutagenesis level. Therefore, it is crucial to precisely characterize factors that influence the pathway choice to better understand genetic stability at replication forks. In yeast, the complex formed by the Rad51 paralogs Rad55 and Rad57 promotes HR and template-switching at stalled replication forks. At DNA double-strand breaks (DSBs), this complex promotes Rad51 filament formation and stability, notably by counteracting the Srs2 anti-recombinase. To explore the role of the Rad55-Rad57 complex in error-free pathways, we monitored the genetic interactions between Rad55-Rad57, the translesion polymerases Polζ or Polη, and Srs2 following UV radiation that induces mostly single-strand DNA gaps. We found that the Rad55-Rad57 complex was involved in three ways. First, it protects Rad51 filaments from Srs2, as it does at DSBs. Second, it promotes Rad51 filament stability independently of Srs2. Finally, we observed that UV-induced HR is almost abolished in Rad55-Rad57 deficient cells, and is partially restored upon Polζ or Polη depletion. Hence, we propose that the Rad55-Rad57 complex is essential to promote Rad51 filament stability on single-strand DNA gaps, notably to counteract the error-prone TLS polymerases and mutagenesis.

46 # Author summary

47 Processive and accurate DNA polymerases replicate genomic DNA during the S phase of
48 each cell cycle. DNA base lesions on template DNA block these polymerases and result in an
49 accumulation of single-stranded DNA gaps behind moving replication forks. These gaps are
50 filled-in by error-prone and error-free pathways. In this work, we show that the complex made
51 by the Rad51 paralogs Rad55 and Rad57 is essential for the error-free homologous
52 recombination gap-filling pathway when DNA replication is stalled by UV-induced DNA
53 lesions, but not for DNA double strand break repair. Interestingly, we found that homologous
54 recombination is efficiently outcompeted by error-prone translesion DNA polymerases in
55 Rad55-Rad57-deficient cells. We propose that the Rad55-Rad57 complex is essential for
56 Rad51 filament stability at UV-induced DNA gaps to promote efficient error-free
57 homologous recombination. Furthermore, our study in yeast predicts that inhibitors of error-
58 prone DNA polymerases might selectively target cancer cells in which RAD51 paralogs are
59 mutated.

Introduction

In all living organisms, genomic DNA undergoes chemical modifications or crosslinking with proteins. These damages greatly compromise DNA replication because they induce replication fork stalling. DNA damage tolerance mechanisms have evolved to ensure completion of genome replication [1], and rely on two main mechanisms: i) translesion synthesis (TLS) DNA polymerases and ii) the use of a homologous template, typically the newly synthesized sister chromatid. Specialized TLS polymerases efficiently insert nucleotides opposite and beyond lesions on DNA templates that block the replicative DNA polymerases [2]. They possibly extend blocked primer/template junctions at replication forks or at single-stranded DNA (ssDNA) gaps left behind the forks [3,4]. TLS polymerases are intrinsically error-prone and constitute a major source of DNA damage-induced mutagenesis [5,6]. Recombination-mediated pathways, such as the template switching and homologous recombination (HR) pathways, mediate damage bypass through the annealing of the damaged ssDNA gaps to the intact homologous template on the sister chromatid [7–9]. HR, also referred to as the salvage pathway, can use homologous chromosomes as intact donors rather than sister chromatids [10]. As TLS, template switching and HR compete for the same ssDNA substrates, they can partly compensate for each other [11–13]. However, template switching and HR are error-free lesion bypass mechanisms and counterbalance mutagenesis induced by TLS [14,15]. Thus, it is crucial to precisely characterize the factors that influence pathway choice to better understand genetic stability at replication forks.

The template switching pathway involves ubiquitin ligase and the Rad18/Rad6 pathway conjugating activities. In budding yeast, Rad6 and Rad18 induce PCNA mono-ubiquitination at its conserved K164 residue, whereas Rad5 and Mms2-Ubc13-dependent activities trigger its poly-ubiquitination at K164 [16,17] and the formation of X-shaped intermediates between

85 sister chromatids when replication is challenged by DNA damages [8]. Interestingly, the
86 formation of these X-shaped intermediates relies also on the HR factors Rad51 and Rad52
87 [7,18].

88 The HR pathway relies on the recombinase Rad51 that oligomerizes on ssDNA to form
89 a right-handed helical nucleoprotein filament [19,20]. This filament performs homology
90 search and catalyzes DNA joint formation between ssDNA and double-stranded DNA
91 (dsDNA) homologous partners, thereby leading to strand exchange [21–23]. Eventually,
92 repair DNA synthesis occurs from the damaged DNA invading ends on undamaged template
93 homologous DNA sequences [24]. Rad51 loading on RPA-coated ssDNA is a crucial step in
94 HR and is mediated mainly by Rad52 in *Saccharomyces cerevisiae* and BRCA2 in metazoans
95 [25–27]. Rad51 filament assembly also requires the activity of Rad51 paralogs (Rad55-Rad57
96 complex in *S. cerevisiae*; RAD51B, RAD51C, RAD51D, XRCC2, and XRCC3 in human
97 cells; and the SHU complex in both [28]). Rad55 and Rad57 share 20% identity with the
98 RecA/Rad51 ATPase core region [29,30]. However, they do not form filaments on ssDNA,
99 and they do not exhibit strand exchange activity [31,32]. Electron microscopy images showed
100 the association of gold-labeled Rad55 with Rad51 filaments assembled on ssDNA (Rad51-
101 ssDNA) [32], and two-hybrid experiments revealed the interaction between Rad51 and Rad55
102 [33,34]. However, recent single-molecule studies suggest that the interaction between the
103 Rad55-Rad57 complex and Rad51 filaments is transient and the Rad55-Rad57 complex
104 dissociates during filament extension [35]. As similar findings were obtained in nematodes
105 [36], it has been proposed that RAD51 paralogs behave as classical chaperones to temporarily
106 assist Rad51 filament formation. More studies are required to clearly describe the precise role
107 of each complex of Rad51 paralogs. In addition, each complex might play a specific role
108 depending on the initial HR-inducing DNA lesion [37].

109 Rad55-Rad57 role in DNA double strand break (DSB) repair is considered accessory
110 on the basis of the weaker sensitivity of *rad55* and *rad57* mutants to ionizing radiation and to
111 site-directed DSBs compared with *rad51* mutants [38,39]. Interestingly, this sensitivity seems
112 to depend on the Srs2 helicase activity because it is partially suppressed by *SRS2* ablation
113 [32,39]. *In vitro* experiments have shown that the Srs2 translocase activity disrupts Rad51
114 filaments [40,41] and that the Rad55-Rad57 complex counteracts Srs2 to maintain Rad51
115 filaments on ssDNA [32,35]. Therefore, it has been proposed that Rad51 filament assembly
116 and disassembly, which are mediated by the Rad55-Rad57 complex and Srs2 respectively,
117 provide a regulatory mechanism to control HR initiation. However, *SRS2* deletion does not
118 rescue spontaneous HR defects between direct repeats in the *rad55* and *rad57* mutants,
119 indicating that the Rad55-Rad57 complex also acts independently of Srs2 [39].
120 To explain the different defects observed between spontaneous and DSB-induced HR,
121 it was hypothesized that spontaneous HR between direct repeats is initiated by ssDNA gaps
122 rather than DSBs [39]. Thus, the Rad55-Rad57 complex would play a more prominent role in
123 HR when the initiating lesion is a ssDNA gap. In agreement, it has been observed that in cells
124 lacking the TLS polymerases Pol ζ, *RAD55* ablation leads to a synergistic increase in DNA
125 damage sensitivity [42–44].
126 Here, we explored Rad55-Rad57 role in Rad51 filament formation on ssDNA gaps and
127 in the balance between HR and TLS in *S. cerevisiae*. For that purpose, we induced
128 interhomolog HR in diploid strains by ionizing radiation (IR) or UV radiation. IR generates
129 DSBs and ssDNA gaps [45], whereas UV generates mostly ssDNA gaps. UV-irradiated *S.*
130 *cerevisiae* cells uncouple leading and lagging strand replication at irreparable UV lesions,
131 thus generating long ssDNA regions on one side of the fork. Furthermore, small ssDNA gaps
132 accumulate along replicated duplexes, likely resulting from repriming events downstream of
133 the lesions on both leading and lagging strands. Translesion synthesis and homologous

134 recombination counteract gap accumulation, without affecting fork progression [11].
135 Recently, RPA foci were used as a read-out of ssDNA gaps forming upon DNA replication
136 through Methyl-methane sulfonate (MMS)- and UV-induced DNA damage [13]. They
137 predominantly form far away from sites of ongoing replication, and they do not overlap with
138 any of the repair centers associated with collapsed replication forks or DNA double-strand
139 breaks. Instead, they represent sites of post-replicative DNA damage bypass involving
140 translesion synthesis and homologous recombination. Therefore, we also used this mark to
141 evaluate the cross-talk between TLS and HR.
142 We found that the Rad55-Rad57 complex is essential for UV-induced HR, but only
143 accessory for IR-induced HR. Interestingly, this essential role is mainly Srs2-independent,
144 and UV-induced HR in Rad55-Rad57-deficient cells can be restored by inactivation of a TLS
145 polymerase (Polζ or Polη). Conversely, UV-induced HR cannot be restored upon inactivation
146 of the template switch pathway in *MMS2* deficient cells. Overall, our results show that the
147 Rad55-Rad57 complex is essential for Rad51 filament assembly on UV-induced ssDNA gaps.
148 When this complex is absent, Rad51 filaments cannot prevent the recruitment of TLS
149 polymerases and counterbalance mutagenesis.
150

151 # Results

152 ## The Rad55-Rad57 heterodimer is essential for UV-induced
153 ## homologous recombination

154 To investigate Rad55-Rad57 role in HR, we analyzed UV- and IR-induced
155 interhomolog HR in wild type (WT) and *rad55*Δ isogenic diploid strains. The previous
156 observation that *rad51* and *rad52* mutant cells are very sensitive to IR indicates that IR
157 generates DSBs, whereas these mutants are much more resistant to UV radiation, indicating
158 that DSBs are probably rarely induced [46,47]. Additionally, genetic evidence suggests that

159 UV-induced HR is triggered by ssDNA gaps [48]. We measured interhomolog HR using two
160 mutant alleles of *ARG4*: *arg4-RV*, a 2-bp deletion that ablates the *Eco*RV site at position
161 +258, and *arg4-Bg*, a 4-bp insertion by fill-in of a *Bgl*II site at position +1,274 [49] (**Fig 1A**).
162 These alleles do not revert [49] and only recombination in heteroallelic *arg4-RV*/*arg4-Bg*
163 diploid cells results in the formation of a WT *ARG4* gene primarily by non-reciprocal transfer
164 covering one mutation [50].

165 The *rad55*Δ diploid strain was not sensitive to UV radiation (**Fig 1B**), but remarkably,
166 UV-induced recombinant [Arg^+] frequency was strongly reduced in the *rad55*Δ diploid strain
167 compared with WT cells (10-fold at 120 J/m^2) (**Fig 1C**). These results are very similar to
168 those previously obtained with *rad51*Δ mutants [46], suggesting that the Rad55-Rad57
169 complex is determinant in UV-induced HR. Conversely, *rad55*Δ diploid cells were sensitive
170 to IR (**Fig 1D**), but γ-ray-induced HR frequencies were identical in *rad55*Δ and WT cells at
171 high doses (400 Gy and 600 Gy) (**Fig 1E**). We observed the same phenotypes in the *rad57*Δ
172 mutant (**S1 Fig A, B, C, D**). Likewise, it was previously reported that spontaneous HR rates
173 are identical in *rad57*Δ and WT cells [38,51], a result we confirmed here in *rad55*Δ cells
174 (**Fig. 1F**). These observations suggest that the Rad55-Rad57 complex plays a specific and
175 essential role in UV-induced HR, probably at ssDNA gaps. This complex is also involved in
176 the repair of IR-induced DSBs, as shown by the lower survival of *rad55*Δ mutant. However, it
177 is not essential since the IR-induced HR frequencies are comparable to WT.
178

179 Resolution of UV-induced RPA foci is delayed in the 180 *rad55*Δ mutant

181 To further examine the role of Rad55 in the management of ssDNA gaps induced by
182 UV exposure, we monitored ssDNA by fluorescence microscopy using YFP-tagged Rfa1, the
183 large subunit of the RPA complex [52]. It was indeed recently established that RPA foci

184 formed upon UV-irradiation represent sites of post-replicative DNA damage bypass involving
185 TLS and HR [13]. Exponentially growing cells were α-factor arrested in G1 and subjected or
186 not to UV irradiation. In absence of irradiation, RPA foci were barely detectable in WT G1-
187 arrested cells (**S1 Fig E)**. After UV-exposure, only a few G1-arrested WT cells displayed
188 RPA foci (3.2% and 12.5% after 60 min and 240 min post-irradiation, respectively; **S1 Fig**
189 **E)**. Unirradiated WT cells released into the cell cycle also exhibit few RPA foci (10% of the
190 cells 60 min after release; **Fig 1H**). In marked contrast, 58% of WT irradiated cells displayed
191 at least one RPA foci 60 min after release in the cell cycle (**Fig 1H**). This confirms that UV-
192 induced DNA damages induced in G1 leads to the formation of ssDNA gaps related to the
193 encounter with DNA replication. Most of UV-induced RPA foci (70%) have been resolved
194 240 min after release (**Fig 1G**; **S1 Fig F**). This illustrates the efficient post-replicative DNA
195 damage bypass in WT cells.

196 Surprisingly, a steady level of 20% of *rad55*Δ G1-arrested cells exhibits RPA foci **(S1**
197 **Fig E**). This rate slowly increases after UV-exposure to reach 60% of G1-arrested cells at 240
198 min (**S1 Fig E**). This newly described phenotype of *rad55*Δ cells is probably representative of
199 an involvement of Rad55-Rad57 in the stabilization of repair intermediates of spontaneous
200 and UV-induced DNA lesions in G1-arrested cells. 60 min after UV-exposure and release in
201 the cell cycle, 80% of *rad55*Δ cells exhibit RPA foci (**Fig 1H**). Moreover, 31% of *rad55*Δ
202 cells display three or more UV-induced RPA foci while this class is observed only in 10% of
203 WT cells. In addition, contrary to WT, only 33% of RPA foci have been resolved 240 min
204 post-irradiation. Finally, we observed an accumulation of *rad55*Δ cells in the second S phase
205 240 min after release from G1 arrest, probably related to the persistence of UV-induced gaps
206 in absence of efficient HR (**S1 Fig F**). Altogether, these results confirm that Rad55-Rad57 is
207 important to manage ssDNA gaps forming upon UV-exposure.

208 In order to confirm that the different behavior of Rad55-Rad57 after UV- and IR-
209 exposure is related to the difference in the lesions induced, we also observed RPA foci
210 formation in WT and *rad55*Δ cells exposed to IR. To allow haploid cells to repair γ-induced
211 DSBs by HR between sister chromatids, cells were irradiated 60 min after their release from
212 the G1 arrest (**S2 Fig A**). In WT and *rad55*Δ cells, we found the same proportion of cells
213 displaying RPA foci after γ-rays exposure compared with UV, these foci being resolved with
214 the same kinetics (**S2 Fig B**). However, as already described in [13], 60 min after irradiation,
215 75% of the γ-irradiated cells with RPA foci display only one focus (**S2 Fig B**), while this
216 class represents 59% of UV-irradiated cells with RPA foci (**Fig 1G**). This difference could be
217 attributed to the formation of a DSB repair center after γ-rays exposure while ssDNA gaps are
218 not gathered after UV-irradiation. This difference is even more pronounced in the *rad55*Δ
219 mutant. Indeed, 76% of γ-irradiated cells with RPA foci show only one focus while this class
220 with a single focus represents 44% of UV-irradiated cells with RPA foci. These differences
221 support our conclusion that Rad51 filament are assembled mainly on ssDNA gaps after UV
222 exposure, while some events might be gathered in repair centers after γ-rays irradiation.
223

224 UV-induced DNA lesions are channeled towards the *REV3* 225 error-prone DNA repair pathway in the *rad55*Δ mutant

226 Although UV-induced HR was almost abolished in *rad55*Δ cells, these cells were
227 resistant to UV radiation. We hypothesized that in *rad55*Δ mutant cells, UV-induced ssDNA
228 gaps at replication forks could be repaired by TLS instead of HR. The TLS polymerase Polζ
229 is required to bypass UV-induced DNA lesions, as illustrated by the strong UV-sensitivity of
230 haploid cells lacking the Rev3 catalytic subunit of Polζ (**Fig 2A**) [54]. Conversely, *rev3*Δ
231 diploid cells were much more resistant to UV radiation (**Fig 2B**), possibly due to HR
232 promoted by *MAT* heterozygosity [51,55–57]. In addition, Polζ, is responsible for almost all

233 UV-induced mutagenesis in yeast cells [54,58], as shown by the absence of UV-induced
234 mutagenesis observed in the Polζ essential component *rev3* mutant [54]. Therefore, *rad55*Δ
235 cells should strongly rely on Polζ and on its catalytic subunit Rev3 for UV resistance, and that
236 UV-induced mutagenesis should increase in *rad55*Δ cells, as previously shown for
237 spontaneous mutagenesis [42]. In agreement with previous studies, we confirmed that UV
238 sensitivity is much higher in the *rev3*Δ *rad55*Δ double mutant than in the *rev3*Δ single
239 mutant in haploid cells [42–44] (**Fig 2A**) and also in diploid cells (**Fig 2B**). This UV
240 sensitivity is comparable with those we previously observed in the *rev3*Δ *rad51*Δ double
241 mutant [59], confirming the essential role of Rad55-Rad57 in UV-induced HR. Therefore, the
242 high resistance to UV of Rad55-deficient cells relies on the TLS pathway that could
243 compensate for HR deficiency in these cells. Consequently, we expected an increase of
244 mutagenesis frequency in *rad55*Δ cells. In agreement with this hypothesis, the frequency of
245 UV-induced canavanine-resistant cells [60] was two-fold higher in the *rad55*Δ mutant than in
246 WT cells (**Fig 2C**). This observation supports the channeling of DNA lesions towards the
247 error-prone Polζ-dependent pathway in *rad55*Δ cells.
248 Measurement of RPA foci in UV-irradiated cells confirmed that TLS can compensate
249 for HR. While the number of RPA foci was about the same in the *rev3*Δ mutant and in the
250 *rad55*Δ mutant (**Fig 1G** and **Fig 2D**), the *rev3*Δ *rad55*Δ double mutant shows RPA foci in
251 almost all cells with 64% of this population displaying at least three foci (**Fig 2D**). We also
252 observed that *rev3*Δ mutants display an accumulation of cells in the second S phase 240 min
253 after release from G1 arrest, while *rev3*Δ *rad55*Δ double mutant shows a block in the first G2
254 phase after the release (**S3 Fig**). The number of cells displaying RPA foci barely decreased
255 with time in *rev3*Δ *rad55*Δ double mutant. However, the number of cells displaying at least
256 three foci decreases strongly, which could represent repair events but also the disappearance
257 of ssDNA gaps through degradation or breakage in the absence of repair. Considering the low

258 survival of UV-irradiated *rev3*Δ *rad55*Δ cells, this more likely indicates that many ssDNA
259 gaps formed during the first S phase after release cannot be repaired in absence of TLS and
260 HR, leading to faulty mitosis. We also observed that the number of spontaneous RPA foci is
261 2-fold higher in the *rad55*Δ *rev3*Δ mutant compared with the *rad55*Δ mutant, indicating a
262 large accumulation of ssDNA gaps related to DNA replication independently of UV-exposure
263 in this double-mutant (compare Fig.1G and 2D).
264

265 UV-induced DNA lesions are channeled to the HR pathway 266 in cells lacking TLS polymerases

267 The finding that UV-induced DNA lesions can be channeled to the TLS pathway in
268 *rad55*Δ cells suggested that such lesions could be managed by the HR pathway in TLS-
269 deficient cells. In that case, TLS-deficient cells should display a hyper-recombinogenic
270 phenotype. To test this hypothesis, we measured the frequencies of UV-induced HR in *rev3*Δ
271 (Polζ mutant) and *rad30*Δ (Polη mutant) cells. As expected, HR frequency was strongly
272 increased in *rev3*Δ cells and to a lower extent in the *rad30*Δ mutant (**Fig 3A and B**).
273 However, UV sensitivity was similar in diploid cells harboring the *rev3*Δ or *rad30*Δ mutation
274 (**Figs 2B and 3C**). We propose that in the *rad30*Δ mutant, UV-induced DNA lesions can be
275 bypassed by both HR and Polζ, while Polη cannot always take over Polζ function in *rev3*Δ
276 cells, resulting in higher HR frequency. Additionally, it is important to note that accordingly
277 with the strong sensitivity of *rev3*Δ cells exposed to UV, HR cannot compensate for all UV-
278 induced DNA lesions that are supported by the TLS pathway.
279

Translesion DNA polymerases prevent UV-induced HR in the *rad55*Δ mutant

We showed that UV-induced HR is strongly decreased in Rad55-Rad57 deficient cells. We also observed that the TLS and HR pathways compete for the same UV-induced ssDNA gaps, because mutagenesis was increased in *rad55*Δ mutants, and HR in *rev3*Δ mutants. Therefore, the recruitment of TLS polymerases at the lesion site might decrease HR in *rad55*Δ cells. We measured HR frequencies and observed a significantly increased frequency in the *rev3*Δ *rad55*Δ double mutant compared with *rad55*Δ cells (**Fig 4A**). This indicated that Polζ effectively impairs HR in the absence of the Rad55-Rad57 complex. We propose that the Rad55-Rad57 complex is important to stabilize Rad51 filaments on ssDNA gaps at the DNA lesion site, thus limiting the recruitment of TLS polymerases. Our results also suggest that in the absence of the Rad55-Rad57 complex, Rad51 filaments are functional enough to promote some HR events (**Fig 4A**), although this is not sufficient to improve UV resistance (**Fig 2**). We observed the same results when a Polη mutation (*rad30*Δ) was combined with *rad55*Δ (**Fig 4B-D**). Thus, both Polζ and Polη contribute to the decrease of UV-induced HR in *rad55*Δ mutant cells.

Next, we asked whether UV-induced HR can be observed independently of the Rad55-Rad57 complex in cells deficient for the template switching pathway. Therefore, we measured the cell survival and recombination frequencies after UV radiation of cells in which *MMS2* was deleted. We found that the *rad55*Δ *mms2*Δ double mutant was more sensitive than the single mutants (**Fig 4E**), suggesting that some template switching events can occur independently of HR. Strikingly, the frequency of UV-induced recombinants was as low in the *rad55*Δ *mms2*Δ double mutant as in the *rad55*Δ mutant (**Fig 4F**). This suggests that the template switching pathway does not compete with HR between homologous chromosome and that TLS polymerases still prevent HR in the *rad55*Δ *mms2*Δ double mutant. On the

305 other hand, the recombination frequency in the *mms2*Δ single mutant was increased, but only
306 after exposure to the highest UV dose (120 J/m^2, **Fig 4F**).
307

308 The acute UV sensitivity of the *rad55*Δ *rev3*Δ double 309 mutant is partially suppressed by *SRS2* deletion

310 As the Rad55-Rad57 complex limits Rad51 filament destabilization by Srs2 at DSBs
311 [32,35], we asked whether Srs2 would be involved in the defective UV-induced HR
312 associated with *rad55*Δ or *rad57*Δ. To address this question, we measured UV-induced HR
313 frequencies in *rad55*Δ *srs2*Δ and *rad57*Δ *srs2*Δ double mutants. We found that they were
314 similar to those observed in *rad55*Δ and *rad57*Δ single mutants (**Fig 5A and B**; **S4 Fig A**
315 **and B**). However, *rev3*Δ *rad55*Δ *srs2*Δ diploid cells were less sensitive to UV radiation than
316 *rev3*Δ *rad55*Δ cells (**Fig 5C**). Thus, the Rad55-Rad57 complex is also involved in the
317 protection of Rad51 filaments against Srs2 at ssDNA gaps formed after UV radiation, but this
318 can only be seen in the absence of Polζ. When Polζ is active, the HR rate is probably too low
319 in *rad55*Δ mutant cells to allow the detection of the effect of Rad51 displacement by Srs2.
320 Additionally, the level of resistance conferred by the deletion of *SRS2* in *rad55*Δ *rev3*Δ cells
321 do not reach those of the *rev3*Δ single mutant (**Fig 5C**). This indicates that the Rad55-Rad57
322 complex plays a Srs2-independent role in UV-induced HR that is only revealed in *rev3*Δ
323 mutants. We propose that the Rad55-Rad57 complex provides stability to Rad51 filaments
324 independently of the protection against Srs2.
325 To sustain our conclusion, we analyzed UV-induced RPA foci in *srs2*Δ cells. The
326 resolution of UV-induced RPA foci is delayed in *srs2*Δ cells compare to WT but in a lesser
327 extent than in *rad55*Δ cells (**Figs 1G and 5E**). Moreover, the delay in UV-induced RPA foci
328 resolution observed in the *rad55*Δ single mutant (**Fig 1G; S1 Fig F**) is the same than in the
329 *rad55*Δ *srs2*Δ double mutant (**Fig 5F; S5 Fig**), suggesting that the antirecombinase activity of

330 Srs2 does not account for the delay observed in the *rad55*Δ mutant. Similarly, the number of
331 spontaneous and UV-induced RPA foci observed in *rev3*Δ *rad55*Δ *srs2*Δ haploid cells was
332 the same as the number observed in the *rev3*Δ *rad55*Δ double mutant **(Fig 5F).** Moreover, the
333 absence of Srs2 does not suppress the block in the first G2 phase after the release observed in
334 the *rev3*Δ *rad55*Δ double mutant following UV irradiation (**S3 Fig; S5 Fig**).
335

336 The Rad55-Rad57 complex is essential for the formation of 337 UV-induced lethal recombination events

338 We confirmed that the *srs2*Δ diploid strain is very sensitive to UV radiation as reported
339 before [61]; however, this sensitivity was completely suppressed in *rad55*Δ *srs2*Δ and
340 *rad57*Δ *srs2*Δ mutant cells (**Fig 5D**; **S4C Fig**). Previous genetic studies led to the concept of
341 toxic Rad51-dependent recombination intermediates that accumulate in the absence of Srs2
342 [62–64]. Therefore, on the basis of the complete suppression of *srs2*Δ-associated UV
343 sensitivity by *rad55*Δ and *rad57*Δ, we propose that the Rad55-Rad57 complex participates in
344 the formation of UV-induced Rad51 filaments that are toxic for the cells in the absence of
345 Srs2. In agreement with previous reports [61,65,66], we observed a strong UV-induced hyper-
346 recombination phenotype in Srs2-deficient cells. This phenotype was completely suppressed
347 by the concomitant deletion of Rad55 or Rad57 (**Fig 5A**; **S4A Fig**).
348

349 The translesion DNA polymerases Polζ and Polη are not 350 essential for DSB repair

351 The large impact of the *rad55*Δ *rev3*Δ double mutant on cell survival after UV radiation
352 suggested that the Rad55-Rad57 complex and Polζ play an important and specific role in UV-
353 induced DNA repair. Although the Rad55-Rad57 complex is not essential for DSB repair
354 [39], we wanted to determine the potential role of TLS polymerases in DSB repair in *rad55*Δ

355 cells. To this aim, we measured the repair of a DSB induced at the *MAT* locus upon
356 expression of the HO endonuclease controlled by a galactose-inducible promoter. The DSB
357 was repaired by HR using an ectopic *MAT***a**-inc sequence inserted in chromosome V [66,67]
358 (**Fig 6A**). After DSB induction, survival was decreased by 3-fold in *rad55*Δ cells compared
359 with WT cells (**Fig 6B**). Conversely, survival of the *rev3*Δ, *rad30*Δ, and *rev3*Δ *rad30*Δ
360 mutants was not affected by DSB induction, and they did not change the sensitivity of the
361 *rad55*Δ mutant. This indicates that the TLS polymerases are not required for DSB repair
362 efficiency.
363

364 # Discussion

365 ## The Rad55-Rad57 complex is essential for HR-mediated
366 repair of UV-induced ssDNA gaps

367 Genetic studies provided evidence that ssDNA gaps are the major initiator of
368 spontaneous and UV-induced HR in yeast [47,57]. In addition, electron microscopy and two-
369 dimensional gel electrophoresis showed that UV-irradiated cells accumulate ssDNA gaps,
370 likely resulting from re-priming events downstream of stalled replication forks at UV-induced
371 DNA lesions [11]. UV-induced ssDNA gaps were also inferred from a physical assay [12]
372 and from the study of RPA foci distribution relatively to sites of ongoing replication [13].
373 Interestingly, both studies reported that TLS and HR counteract ssDNA gap accumulation.
374 Here, we show that the complex formed by the Rad51 paralogs Rad55 and Rad57 is
375 essential for UV-induced ssDNA gaps repair, while accessory at DSB sites. We observed a
376 strong decrease of HR frequencies in the *rad55*Δ and *rad57*Δ mutants specifically after UV
377 radiation. Moreover, we confirmed the synergistic increase of UV sensitivity upon depletion
378 of both Rad55 and Polζ in haploid and diploid cells (**Fig 2A and B**). This was confirmed by
379 the large increase in the number of UV-induced RPA foci observed in the *rad55*Δ *rev3*Δ

380 double mutant (**Fig 2D**). We did not observe this negative interaction after induction of a site-
381 directed DSB (**Fig 6**). In addition, we found that UV-induced mutagenesis at the *CAN1* locus
382 was increased in the *rad55*Δ mutant (**Fig 2C**), and that UV-induced HR was increased in Pol
383 ζ and Pol η deficient cells (**Fig 3A and B**). Most importantly, we observed UV-induced HR
384 in the absence of the Rad55-Rad57 complex only in cells deficient for TLS (**Fig 4**). These
385 data suggest that the Rad55-Rad57 complex might stabilize Rad51 filaments on ssDNA gaps
386 to prevent the recruitment of the TLS polymerases.
387

388 The Rad55-Rad57 complex plays three prominent roles in 389 UV-induced HR

390 One of the best defined role of Rad55-Rad57 is the protection of Rad51 filaments from
391 Srs2 at DSBs [32,35]. Here, we found that although the defect in UV-induced HR observed in
392 *rad55*Δ cells was not suppressed by *SRS2* deletion **(Fig 5A and B)**, the very high UV
393 sensitivity of the *rad55*Δ *rev3*Δ double mutant was partially suppressed by *srs2*Δ (**Fig 5C**).
394 This suggests that the Rad55-Rad57 complex protects Rad51 filaments against Srs2 also at
395 UV-induced ssDNA gaps, although Esc2- and Elg1-dependent mechanisms also regulate
396 negatively Srs2 at sites of stalled replication forks [68,69]. Additional studies are required to
397 determine the interplay between these regulating factors.
398 The increased UV-sensitivity of the *rev3*Δ *rad55*Δ *srs2*Δ triple mutant compared with
399 the *rev3*Δ single mutant (**Fig 5C**) clearly indicates that the Rad55-Rad57 complex plays a
400 Srs2-independent role in UV-induced HR. We propose that the second role of this complex is
401 to provide stability to Rad51 filaments, independently of the protection against Srs2. In
402 agreement with this conclusion, we found that in *rad55*Δ or *rad57*Δ mutants, *srs2*Δ-
403 associated UV-sensitivity was completely suppressed (**Fig 5D, S4C Fig**). This indicates that
404 in the absence of Srs2 activity, Rad51 stabilization by the Rad55-Rad57 complex would lead

405 to lethal events, possibly initiated by ssDNA gaps that could block replication fork restart. On
406 the basis of the results of single-molecule studies, it was proposed that the Rad55-Rad57
407 complex helps Rad51 filament formation by acting as a chaperone [35], in agreement with our
408 observations.

409 Remarkably, UV-induced HR frequency increased in *rad55*Δ cells upon Polζ or Polη
410 deletion (**Fig 4**). Therefore, the third role of the Rad55-Rad57 complex would be to allow HR
411 to outcompete the TLS polymerases. Rad51 filament stabilization by the Rad55-Rad57
412 complex on ssDNA at the lesion site could prevent the recruitment of TLS polymerases by
413 PCNA because of structural constraints. In the absence of Rad55-Rad57, unstable Rad51
414 filaments cannot prevent the loading of the TLS polymerases that inhibit HR and induce
415 mutagenesis. TLS polymerase depletion in *rad55*Δ mutants would allow some HR events to
416 occur, but the inherent instability of Rad51 filaments would make them rare and explain the
417 low survival rate of *rev3*Δ *rad55*Δ mutant cells. Our results clearly highlight that UV-induced
418 lesions can be channeled from HR to TLS and *vice versa*, when one pathway is inactivated.
419 This provides further support to a model in which HR and TLS can share common substrates
420 [12,13].
421

422 Model for the activity of the Rad55-Rad57 complex in 423 ssDNA gap repair

424 Our genetic data suggest three different and essential functions for the Rad55-Rad57
425 complex in UV-induced interhomolog HR initiated at ssDNA gaps (**Fig 7A**). First, this
426 complex is required for Rad51 filament formation and stabilization that are essential for
427 efficient strand exchange at ssDNA gaps. The 5'ends of DSBs are resected to generate 3'
428 ssDNA that can invade the homologous donor. Conversely, 3' ssDNA is not directly available
429 at ssDNA gaps. Therefore, the Rad55-Rad57 complex may be required to form Rad51

430 filaments that can invade without 3' ssDNA extremities. Alternatively, the Rad55-Rad57
431 complex can be involved in the 3' end denaturation at the lesion site to generate a 3' ended
432 ssDNA by recruitment of a DNA helicase. Second, the Rad55-Rad57 complex within Rad51
433 filaments counterbalances Srs2 activity through a mechanism that remains poorly understood
434 [32,35]. Third, the Rad55-Rad57 complex could inhibit TLS polymerases by limiting their
435 loading at the primer/template junction within ssDNA gaps, probably through the stabilization
436 of Rad51 filaments (**Fig 7B-E**). This competition might be crucial to control mutagenesis
437 resulting from gap-filling by Polζ, but further studies will be required to understand how the
438 access of HR and TLS are regulated at the site of lesions and to determine the nature of the
439 lesions that can only be managed by TLS, as shown by the acute sensitivity of UV-irradiated
440 *rev3*Δ mutant. Thus, in our model, Rad51 filaments formed with the Rad55-Rad57 complex
441 preserve the genome stability through ssDNA gap repair by HR, but also through competition
442 with TLS on common ssDNA gap substrates.
443

444 The interplay between HR and TLS in mammals

445 The interplay between error-prone and error-free lesion-bypass pathways is documented
446 in *E. coli* and yeast (the present study, [13,14]), and it has been recently investigated in
447 mammals. First of all, it was recently shown that BRCA-deficient tumors sensibility to
448 cisplatin and synthetic lethality with PARP inhibitors were associated with a BRCA default in
449 preventing replication-associated gaps rather than in preventing DSBs [70,71]. More
450 specifically, HR can be triggered by PRIMPOL-dependent ssDNA gaps behind stalled
451 replication forks [72]. Moreover, BRCA1- and BRCA2-defective breast cancer cells, display
452 an increased somatic mutational load specific of TLS polymerases [73–76]. Accordingly, a
453 recent study found that BRCA1/2-defective cancer cells rely much more on TLS for repair of
454 PRIMPOL-dependent ssDNA gaps [77]. In addition, similarly to PARP1 or DNA polymerase

455 Polθ inhibitors that are used to treat HR-deficient cancers [78–80], the small molecule JE-
456 RH-06 disrupts the interaction between the TLS polymerases REV1 and Polζ and shows
457 preferential cytotoxicity in BRCA1-deficient cancer cells [77,81]. Thus, it would be
458 interesting to determine whether the association of cancer-associated RAD51 paralog
459 mutations and TLS mutations leads to a synergic sensitivity to replication fork blocking
460 lesions, as we observed in yeast in the *rad55*Δ *rev3*Δ double mutant. If an acute sensitivity is
461 found, one might expect a cytotoxicity associated with TLS polymerase inhibitors in RAD51
462 paralog-deficient cancer cells.

463 # Materials and Methods

464 ## Yeast strains, plasmids and media

465 The *S. cerevisiae* strains used in the present study are isogenic derivatives of FF18733
466 (*his7-2, leu2-3,112, lys1-1, trp1-289, ura3-52*) and JKM146 (*hml::ADE1 MATalpha*
467 *hmr::ADE1*, *arg5,6::MATa-inc::HPH1*, *ade3::GAL::HO*) and are listed in **S1 Table**. Yeast
468 cells were incubated at 30°C for all the experiments described. Gene deletions were
469 performed by PCR-mediated one-step replacement [82,83]. Mutants were selected on YPD
470 medium containing 300 mg/L geneticin (Sigma) or nourseothricin (cloNAT; Werner
471 BioAgents). All deletions were confirmed by PCR amplification of genomic DNA. All media
472 were prepared as previously described [84].
473

474 ## Irradiation, cell survival assay, and measurement of DNA
475 ## damage-induced HR frequency

476 Cells in stationary phase and in exponential growth phase were used for irradiation
477 with UV and γ-rays, respectively. UV irradiation was performed using a 264 nm source.
478 Yeast cells were irradiated with 30, 60, 90 and 120 J/m^2 (2 J/m^2/s dose rate). γ-irradiation was
479 performed using a GSR D1 irradiator (Gamma-Service Medical GmbH). It is a self-shielded
480 irradiator with four sources of ^{137}Cesium. The total activity was 180.28 TBq in March 2014.
481 As yeast cells resuspended in 1 mL of sterile H_2O were irradiated in 1.5ml plastic microtubes,
482 dosimetry was performed using plastic microtubes with a cylindrical ionizing chamber 31010
483 (PTW, Freiburg, Germany) following the American Association of Physicists in Medicine
484 recommendations [85]. This ionizing chamber has a cavity of 0.125 cm^3 calibrated with
485 ^{137}Cesium in air kerma free in air and the reference number of our facility is 210382401. The
486 polarity and the ion recombination were measured for this ^{137}Cesium source. Each

487 measurement was corrected with the KTP factor to take into account the variations in
488 temperature and atmospheric pressure. Yeast cells were irradiated at 100, 200, 400 and 600
489 Gy (single doses) and with a 12 Gy/min dose rate that takes the radioactive decrease into
490 account.

491 Before (UV) or after (γ-rays) irradiation, cells were plated at the appropriate dilution
492 on rich medium (YPD) to measure the survival rate, and on synthetic plates without arginine
493 to quantify the number of HR events between *ARG4* heteroalleles. HR frequencies were
494 determined by dividing the number of recombinant colonies growing on selective medium by
495 the number of unselected colonies subjected to the same dose of irradiation. The values
496 obtained were corrected by subtracting the number of recombinants on the non-irradiated
497 plates. The mean percentage from at least three independent experiments is presented.
498

499 Measurement of spontaneous heteroallelic HR

500 Rates of spontaneous HR between two heteroalleles of *ARG4* were determined by
501 fluctuation tests using the method of the median [86]. The reported rates were obtained from
502 three independent experiments, each performed with nine independent 2-ml cultures started
503 with less than 200 cells and incubated at 30°C for three days. The significance of the rates is
504 indicated by the 95% confidence interval [86].
505

506 Measurement of UV-induced mutagenesis

507 UV-induced mutagenesis was measured with the *CAN1* forward-mutation assay [60].
508 UV-induced mutagenesis frequencies were obtained by dividing the number of colonies
509 growing on synthetic plates without arginine and containing l-canavanine (Sigma, 30 mg/l)
510 (*i.e.*, canavanine-resistant, Can^R, cells) by the number of cells that survived irradiation
511 counted on rich media YPD. The number of Can^R colonies obtained after irradiation was

512 corrected by subtracting the number of spontaneous Can^R colonies growing on non-irradiated
513 plates.
514

515 Cell growth, synchronization and irradiation before 516 microscopy

517 Cells were grown at 30°C in synthetic complete medium (Formedium). Before UV-
518 and γ-irradiation, growing cells were synchronized in G1 using 17 mg/ml α-factor for 180
519 min. They were released from the G1 arrest by three consecutive washes with sterile H_2O.
520 Cells were resuspended in 50 ml of sterile H_2O and UV-irradiated in a glass plate of diameter
521 190 mm. UV irradiation was performed using a 264 nm source. Yeast cells in water were
522 irradiated with 60 J/m2 (2 J/m2/s dose rate) then resuspended in fresh complete medium. γ-
523 irradiation was performed as described for survival studies. Cells were then resuspended in
524 fresh complete medium. Time-course experiment were started with yeast cultures adjusted to
525 OD_{600} 0.5.
526

527 Microscopy

528 Live-cell images were acquired using a wide-field inverted microscope (Leica DMI-
529 6000B) equipped with Adaptive Focus Control to eliminate Z drift, a 100×/1.4 NA immersion
530 objective with a Prior NanoScanZ Nanopositioning Piezo Z Stage System, a CMOS camera
531 (ORCA-Flash4.0; Hamamatsu) and a solid-state light source (SpectraX, Lumencore). The
532 system is piloted by MetaMorph software (Molecular Device).
533 YFP images were acquired at indicated time points after alpha factor block release and
534 UV or γ-rays irradiation; 19 focal steps of 0.20 µm were acquired with an exposure time of
535 100 ms using a solid-state 500-nm diode and a YFP filter (excitation 470–510 nm and
536 dichroic 495 nm; Chroma Technology Corp.). A single bright-field image on one focal plane

537 was acquired at each time point with an exposure of 50ms. All the images shown are z
538 projections of z-stack images. Image analysis was achieved following processing with ImageJ
539 software (National Institutes of Health), using scripts written in ImageJ macro language.
540 Bright-field and maximum intensity projections of YFP images were merged, Rfa1-YPD foci
541 were then quantified in 2D.
542

543 Measure of DNA content by flow cytometry

544 1 ml of cells were resuspended in 70% Ethanol and kept at 4°C. Cells were
545 centrifuged for 3 min at 7,000 RPM and washed once in PBS, resuspended in PBS with
546 RNase A (0.5 mg/ml) for 2 hours at 50°C. Cells were centrifugated and resuspended in PBS
547 with iodure propidium (50 μg/ml) for one hour at room temperature. Cells were diluted 10-
548 fold in PBS and cell aggregates were dissociated by sonication. DNA content analysis was
549 performed using LSRII flow cytometer (BD Biosciences) and analyzed with the FlowJo
550 software.
551
552

553 Survival following DSB formation

554 Cells were grown overnight in liquid culture medium containing lactate acid instead of
555 glucose. Survival following HO-induced DSB was measured as the number of cells growing
556 on galactose-containing medium divided by the number of colonies growing on YPD. The
557 results shown are the mean values of at least 3 independent experiments.
558
559
560
561

562 # Acknowledgments

563 We thank Jim Haber and Pablo Radicella, for critical and careful reading of the manuscript.
564 We thank Véronique Ménard from the radiation facility of our institute for her help with the
565 use of the GSRD1 irradiator. We also appreciate the help of Elisabetta Andermarcher with the
566 English editing.

567

568

569 # Figure legend

570 **Fig 1. Rad55 plays a major role in UV-induced HR.** (A) Schematic representation of the
571 genetic system used. Frameshift mutations were introduced at the *Eco*RV site (RV, ±2 bp) or
572 the *Bgl*II site (Bg, +4 bp). HR between the two *ARG4* mutant alleles can restore a WT *ARG4*
573 allele associated with the [Arg+] phenotype. (B) Survival and (C) [Arg+] recombinant
574 frequencies after UV exposure of WT and *rad55*Δ diploid cells. (D) Survival and (E) [Arg+]
575 recombinant frequencies after γ irradiation of WT and *rad55*Δ diploid cells. (F) Spontaneous
576 mitotic [Arg+] recombinant rates ([Arg+] x 10^{-7}/cell/generation) of WT and *rad55*Δ diploid
577 strains. (G) Experimental scheme for microscopy analysis of RPA foci: Cells arrested in G1
578 phase with alpha-factor (αF) were exposed to UV before release into the cell cycle. Samples
579 were collected for analysis every hour for four hours. Representative images of Rfa1-YFP
580 cells are presented. Scale bars are 2 μm. (H) Quantification of Rfa1-YFP foci detected by
581 fluorescence microscopy in WT and *rad55*Δ cells exposed or not to UV. Error bars indicate
582 SDs from three independent experiments.

583

584 **Fig 2. Channeling UV-induced DNA lesions into the *REV3*-dependent pathway in**
585 ***rad55*Δ cells.** (A) Survival of haploid cells following UV radiation. (B) Survival of diploid

586 cells following UV radiation. (C) UV-induced mutagenesis in WT and *rad55*Δ cells
587 determined by quantifying the Can^R mutant frequency for the indicated UV doses. (D)
588 Quantification of Rfa1-YFP foci detected by fluorescence microscopy in *rev3*Δ and *rad55*Δ
589 *rev3*Δ cells not irradiated or after UV exposure. Error bars indicate SDs from three
590 independent experiments.
591
592 **Fig 3. Channeling UV-induced DNA lesions into the HR pathway in TLS-deficient cells.**
593 (A) UV-induced [Arg+] recombinant frequencies in WT and *rev3*Δ diploid cells. (B) UV-
594 induced [Arg+] recombinant frequencies in WT and *rad30*Δ diploid cells. (C) Survival of
595 diploid *rad30*Δ cells after UV radiation.
596
597 **Fig 4. *RAD55*-independent UV-induced HR in TLS-deficient cells.** (A) UV-induced
598 [Arg+] recombinant frequencies in *rad55*Δ *rev3*Δ diploid cells. The very strong UV
599 sensitivity displayed by the double mutant precluded the quantification of the UV-induced
600 recombinant rate at UV doses higher than $40J/m^2$. (B) Survival of *rad55*Δ *rad30*Δ diploid
601 cells following UV radiation. (C) UV-induced [Arg+] recombinant frequencies in *rad55*Δ and
602 *rad30*Δ diploids cells. (D) Close-up view of (C) to exclude the hyper-recombinogenic
603 phenotype of *rad30*Δ. (E) *Rad55*Δ *mms2*Δ diploid cell-survival upon UV radiation. (F) UV-
604 induced [Arg+] recombinant frequencies in *rad55*Δ and *mms2*Δ diploid cells.
605
606 **Fig 5. Srs2 role in the *rad55*Δ mutant exposed to UV radiation.** (A) UV-induced [Arg+]
607 recombinant frequencies in *rad55*Δ *srs2*Δ diploid cells. (B) Close-up view of (A) to exclude
608 the hyper-recombinogenic phenotype of *srs2*Δ. (C) The acute UV sensitivity displayed by the
609 *rad55*Δ *rev3*Δ mutant is partially suppressed by *SRS2* deletion. The red arrow between the
610 *rev3*Δ *rad55*Δ and *rev3*Δ *rad55*Δ *srs2*Δ survival curves highlights the partial *srs2*Δ

611 suppression. (D) Survival curves of diploid cells following UV radiation. The acute
612 sensitivity to UV radiation of the diploid *srs2*Δ strain is suppressed by *rad55*Δ (blue arrow).
613 (E) Quantification of Rfa1-YFP foci detected by fluorescence microscopy in *srs2*Δ cells not
614 irradiated or after UV exposure. (F) Quantification of Rfa1-YFP foci detected by fluorescence
615 microscopy in *rad55*Δ *srs2*Δ and *rad55*Δ *rev3*Δ *srs2*Δ cells not irradiated or after UV
616 exposure. Error bars indicate SDs from three independent experiments.
617
618 **Fig 6. TLS DNA polymerases are not required for cell survival after a site-specific DSB.**
619 (A) Schematic representation of the system used to measure repair of a HO-induced DSB by
620 gene conversion between ectopic copies of *MAT*. (B) Cell viability after DSB formation.
621
622 **Fig 7. Model of Rad55-Rad57 roles in the repair of ssDNA gaps by HR behind**
623 **replication forks.** The figure shows an ssDNA gap generated after stalling of a replicative
624 DNA polymerase at a UV-induced DNA lesion. This gap is a substrate for both the HR and
625 TLS pathways. (**A**) The three roles of the Rad55-Rad57 complex in Rad51 filament formation
626 on ssDNA gaps are highlighted: (1) formation of functional Rad51 filaments; (2) protection
627 against Srs2 dismantling activity; (3) prevention of TLS polymerase recruitment at the
628 primer/template junction. (**B**) In WT cells, Rad55-Rad57 heterodimers form and stabilize
629 Rad51 filaments on ssDNA leading to HR, avoiding bypass by TLS. Rad51 filaments could
630 prevent the recruitment of the TLS polymerases Polζ and Polη (collectively named TLS Pol)
631 by covering the 3' extremity blocked at the DNA lesion. (**C**) In the *rad55*Δ mutant, inefficient
632 and/or fewer Rad51 filaments are formed that cannot prevent the recruitment of the TLS
633 polymerases. Therefore, more UV-induced DNA lesions are channeled towards the TLS
634 pathway (bold arrow). (**D**) In the *rev3*Δ or in the *rad30*Δ mutant, the absence of Polζ or Polη
635 allows channeling UV-induced DNA lesions towards the HR pathway (bold arrow). (**E**) In the

636 *rad55*Δ *rev3*Δ and *rad55*Δ *rad30*Δ double mutants both the HR and the TLS pathways are
637 impaired.
638

639 Supporting information

640 **S1 Fig. Rad57 plays a major role specifically in UV-induced HR.** (A) Survival, and (B)
641 [Arg+] recombinant frequencies in WT and *rad57*Δ diploid cells following UV radiation. (C)
642 Survival and (D) [Arg+] recombinant frequencies in WT and *rad57*Δ diploid cells after γ
643 irradiation. (E) Quantification of Rfa1-YFP foci in WT and *rad55*Δ cells not irradiated or
644 after UV exposure in G1-arrested cells. Error bars indicate SDs from three independent
645 experiments. (F) Representative images of Rfa1-YFP WT and r*ad55*Δ cells released from G1
646 arrest and UV-irradiated or not. Bright-field (BF) images are merged with YFP images. Scale
647 bars are 2 μm. FACS profiles for each corresponding time point are shown.
648

649 **S2 Fig. γ-rays-induced RPA foci in WT and *rad55*Δ strains.** (A) Experimental scheme:
650 Cells arrested in G1 phase with alpha-factor (αF) were release into the cell cycle. After one
651 hour from the release, cells were exposed to γ-rays. Samples were collected every hour for
652 four hours. (B) Quantification of Rfa1-YFP foci in WT and *rad55*Δ cells not irradiated or
653 after γ-rays irradiation. Error bars indicate SDs from three independent experiments.
654

655 **S3 Fig. UV-induced RPA foci in the *rev3*Δ and *rad55*Δ *rev3*Δ strains.** Representative
656 images of Rfa1-YFP *rev3*Δ and *rad55*Δ *rev3*Δ cells after release from G1 arrest and UV
657 irradiated or not. Bright-field (BF) images are merged with YFP images. Scale bars are 2 μm.
658 FACS profiles for each corresponding time point are shown.
659
660
661

662 **S4 Fig. Srs2 roles in the *rad57*Δ mutant exposed to UV radiation.** (A) UV-induced [Arg+]
663 recombinant frequencies in *rad57*Δ *srs2*Δ diploid cells. (B) Close-up view of (A) to exclude
664 the hyper-recombinogenic phenotype of *srs2*Δ. (C) Survival curves of diploid cells following
665 UV radiation. The acute sensitivity to UV radiation of the diploid *srs2*Δ strain is suppressed
666 by *rad57*Δ (blue arrow).

667
668 **S5 Fig. RPA foci in *rad55*Δ *rev3*Δ *srs2*Δ cells.** Representative images of Rfa1-YFP *srs2*Δ,
669 *rev3*Δ *srs2*Δ and *rad55*Δ *rev3*Δ *srs2*Δ cells after release from G1 arrest and UV irradiated or
670 not. Bright-field (BF) images are merged with YFP images. Scale bars are 2 μm. FACS
671 profiles for each corresponding time point are shown.

672
673

674
675
676
677
678

679
680 # References

681 1. Branzei D, Psakhye I. DNA damage tolerance. Curr Opin Cell Biol. 2016;40: 137–144.
682 doi:https://doi.org/10.1016/j.ceb.2016.03.015
683 2. Zhao L, Todd Washington M. Translesion synthesis: Insights into the selection and
684 switching of DNA polymerases. Genes. 2017. doi:10.3390/genes8010024
685 3. Lehmann AR, Fuchs RP. Gaps and forks in DNA replication: Rediscovering old
686 models. DNA Repair (Amst). 2006;5: 1495–1498. doi:10.1016/j.dnarep.2006.07.002
687 4. Hedglin M, Benkovic SJ. Eukaryotic Translesion DNA Synthesis on the Leading and
688 Lagging Strands: Unique Detours around the Same Obstacle. Chemical Reviews. 2017.
689 doi:10.1021/acs.chemrev.7b00046

690 5. Waters LS, Minesinger BK, Wiltrout ME, D'Souza S, Woodruff R V, Walker GC.
691 Eukaryotic translesion polymerases and their roles and regulation in DNA damage
692 tolerance. Microbiol Mol Biol Rev. 2009;73: 134–154. doi:10.1128/MMBR.00034-08
693 6. Makarova A V, Stodola JL, Burgers PM. A four-subunit DNA polymerase ζ complex
694 containing Pol δ accessory subunits is essential for PCNA-mediated mutagenesis.
695 Nucleic Acids Res. 2012;40: 11618–11626. doi:10.1093/nar/gks948
696 7. Liberi G, Maffioletti G, Lucca C, Chiolo I, Baryshnikova A, Cotta-Ramusino C, et al.
697 Rad51-dependent DNA structures accumulate at damaged replication forks in sgs1
698 mutants defective in the yeast ortholog of BLM RecQ helicase. Genes Dev. 2005;19:
699 339–350. doi:10.1101/gad.322605
700 8. Branzei D, Vanoli F, Foiani M. SUMOylation regulates Rad18-mediated template
701 switch. Nature. 2008. pp. 915–920. doi:10.1038/nature07587
702 9. Branzei D, Szakal B. DNA damage tolerance by recombination: Molecular pathways
703 and DNA structures. DNA Repair (Amst). 2016;44: 68–75.
704 doi:10.1016/j.dnarep.2016.05.008
705 10. Carr AM, Lambert S. Replication stress-induced genome instability: The dark side of
706 replication maintenance by homologous recombination. Journal of Molecular Biology.
707 2013. pp. 4733–4744. doi:10.1016/j.jmb.2013.04.023
708 11. Lopes M, Foiani M, Sogo JM. Multiple mechanisms control chromosome integrity
709 after replication fork uncoupling and restart at irreparable UV lesions. Mol Cell.
710 2006;21: 15–27. doi:10.1016/j.molcel.2005.11.015
711 12. Ma W, Westmoreland JW, Resnick MA. Homologous recombination rescues ssDNA
712 gaps generated by nucleotide excision repair and reduced translesion DNA synthesis in
713 yeast G2 cells. Proc Natl Acad Sci U S A. 2013;110. doi:10.1073/pnas.1301676110
714 13. Wong RP, García-Rodríguez N, Zilio N, Hanulová M, Ulrich HD. Processing of DNA

715 Polymerase-Blocking Lesions during Genome Replication Is Spatially and Temporally
716 Segregated from Replication Forks. Mol Cell. 2020;77: 3-16.e4.
717 doi:10.1016/j.molcel.2019.09.015
718 14. Fujii S, Isogawa A, Fuchs RP. Chronological switch from translesion synthesis to
719 homology- Dependent gap repair in vivo. Toxicol Res. 2018;34: 297–302.
720 doi:10.5487/TR.2018.34.4.297
721 15. Masłowska KH, Laureti L, Pagès V. iDamage: a method to integrate modified DNA
722 into the yeast genome. Nucleic Acids Res. 2019;47: e124. doi:10.1093/nar/gkz723
723 16. Hoege C, Pfander B, Moldovan G-L, Pyrowolakis G, Jentsch S. RAD6-dependent
724 DNA repair is linked to modification of PCNA by ubiquitin and SUMO. Nature.
725 2002;419: 135–141. doi:10.1038/nature00991
726 17. Torres-Ramos CA, Prakash S, Prakash L. Requirement of RAD5 and MMS2 for
727 Postreplication Repair of UV-Damaged DNA in Saccharomyces cerevisiae. Mol Cell
728 Biol. 2002;22: 2419–2426. doi:10.1128/MCB.22.7.2419-2426.2002
729 18. Vanoli F, Fumasoni M, Szakal B, Maloisel L, Branzei D. Replication and
730 recombination factors contributing to recombination-dependent bypass of DNA lesions
731 by template switch. PLoS Genet. 2010;6: e1001205. doi:10.1371/journal.pgen.1001205
732 19. Conway AB, Lynch TW, Zhang Y, Fortin GS, Fung CW, Symington LS, et al. Crystal
733 structure of a Rad51 filament. Nat Struct Mol Biol. 2004;11: 791–796.
734 doi:10.1038/nsmb795
735 20. Short JM, Liu Y, Chen S, Soni N, Madhusudhan MS, Shivji MKK, et al. High-
736 resolution structure of the presynaptic RAD51 filament on single-stranded DNA by
737 electron cryo-microscopy. Nucleic Acids Res. 2016;44: 9017–9030.
738 doi:10.1093/nar/gkw783
739 21. San Filippo J, Sung P, Klein H. Mechanism of eukaryotic homologous recombination.

740 Annu Rev Biochem. 2008;77: 229–257.
741 doi:10.1146/annurev.biochem.77.061306.125255
742 22. Bell JC, Kowalczykowski SC. Mechanics and Single-Molecule Interrogation of DNA
743 Recombination. Annu Rev Biochem. 2016;85: 193–226. doi:10.1146/annurev-
744 biochem-060614-034352
745 23. Haber JE. DNA Repair: The Search for Homology. BioEssays. 2018.
746 doi:10.1002/bies.201700229
747 24. Mehta A, Haber JE. Sources of DNA double-strand breaks and models of
748 recombinational DNA repair. Cold Spring Harb Perspect Biol. 2014;6: a016428.
749 doi:10.1101/cshperspect.a016428
750 25. Sung P. Function of yeast Rad52 protein as a mediator between replication protein A
751 and the Rad51 recombinase. J Biol Chem. 1997;272: 28194–28197.
752 doi:10.1074/jbc.272.45.28194
753 26. Mortensen UH, Lisby M, Rothstein R. Rad52. Current Biology. 2009.
754 doi:10.1016/j.cub.2009.06.001
755 27. Carver A, Zhang X. Rad51 filament dynamics and its antagonistic modulators. Semin
756 Cell Dev Biol. 2021;113: 3–13. doi:10.1016/j.semcdb.2020.06.012
757 28. Bonilla B, Hengel SR, Grundy MK, Bernstein KA. RAD51 Gene Family Structure and
758 Function. Annu Rev Genet. Annual Reviews; 2020;54: 25–46. doi:10.1146/annurev-
759 genet-021920-092410
760 29. Kans JA, Mortimer RK. Nucleotide sequence of the RAD57 gene of Saccharomyces
761 cerevisiae. Gene. 1991;105: 139–140. doi:https://doi.org/10.1016/0378-
762 1119(91)90527-I
763 30. Lovett ST. Sequence of the RAD55 gene of Saccharomyces cerevisiae: similarity of
764 RAD55 to prokaryotic RecA and other RecA-like proteins. Gene. 1994;

765 doi:10.1016/0378-1119(94)90362-X
766 31. Sung P. Yeast Rad55 and Rad57 proteins form a heterodimer that functions with
767 replication protein A to promote DNA strand exchange by Rad51 recombinase. Genes
768 Dev. 1997;11: 1111–1121. doi:10.1101/gad.11.9.1111
769 32. Liu J, Renault L, Veaute X, Fabre F, Stahlberg H, Heyer W-D. Rad51 paralogues
770 Rad55–Rad57 balance the antirecombinase Srs2 in Rad51 filament formation. Nature.
771 2011;479: 245–248. doi:10.1038/nature10522
772 33. Hays SL, Firmenich AA, Berg P. Complex formation in yeast double-strand break
773 repair: Participation of Rad51, Rad52, Rad55, and Rad57 proteins. Proc Natl Acad Sci
774 U S A. 1995;92: 6925–6929. doi:10.1073/pnas.92.15.6925
775 34. Johnson RD, Symington LS. Functional differences and interactions among the
776 putative RecA homologs Rad51, Rad55, and Rad57. Mol Cell Biol. 1995;15: 4843–
777 4850. doi:10.1128/MCB.15.9.4843
778 35. Roy U, Kwon Y, Marie L, Symington L, Sung P, Lisby M, et al. The Rad51 paralog
779 complex Rad55-Rad57 acts as a molecular chaperone during homologous
780 recombination. Mol Cell. 2021;81: 1043-1057.e8. doi:10.1016/j.molcel.2020.12.019
781 36. Belan O, Barroso C, Kaczmarczyk A, Anand R, Federico S, O'Reilly N, et al. Single-
782 molecule analysis reveals cooperative stimulation of Rad51 filament nucleation and
783 growth by mediator proteins. Mol Cell. 2021;81: 1058-1073.e7.
784 doi:10.1016/j.molcel.2020.12.020
785 37. Garcin EB, Gon S, Sullivan MR, Brunette GJ, de Cian A, Concordet JP, et al.
786 Differential requirements for the RAD51 paralogs in genome repair and maintenance in
787 human cells. PLoS Genet. 2019;15: 1–29. doi:10.1371/journal.pgen.1008355
788 38. Mozlin AM, Fung CW, Symington LS. Role of the Saccharomyces cerevisiae Rad51
789 paralogs in sister chromatid recombination. Genetics. 2008;178: 113–125.

790 doi:10.1534/genetics.107.082677
791 39. Fung CW, Mozlin AM, Symington LS. Suppression of the double-strand-break-repair
792 defect of the Saccharomyces cerevisiae rad57 mutant. Genetics. 2009;181: 1195–1206.
793 doi:10.1534/genetics.109.100842
794 40. Veaute X, Jeusset J, Soustelle C, Kowalczykowski SC, Le Cam E, Fabre F. The Srs2
795 helicase prevents recombination by disrupting Rad51 nucleoprotein filaments. Nature.
796 2003;423: 309–312. doi:10.1038/nature01585
797 41. Krejci L, Van Komen S, Li Y, Villemain J, Reddy MS, Klein H, et al. DNA helicase
798 Srs2 disrupts the Rad51 presynaptic filament. Nature. 2003;423: 305–309.
799 42. Xu X, Ball L, Chen W, Tian X, Lambrecht A, Hanna M, et al. The yeast Shu complex
800 utilizes homologous recombination machinery for error-free lesion bypass via physical
801 interaction with a Rad51 paralogue. PLoS One. 2013;8: 1–9.
802 doi:10.1371/journal.pone.0081371
803 43. Rattray AJ, Shafer BK, McGill CB, Strathern JN. The roles of REV3 and RAD57 in
804 double-strand-break-repair-induced mutagenesis of Saccharomyces cerevisiae.
805 Genetics. 2002;162: 1063–1077.
806 44. Ball LG, Zhang K, Cobb JA, Boone C, Xiao W. The yeast Shu complex couples error-
807 free post-replication repair to homologous recombination. Mol Microbiol. 2009;73:
808 89–102. doi:10.1111/j.1365-2958.2009.06748.x
809 45. Cadet J, Ravanat J-L, TavernaPorro M, Menoni H, Angelov D. Oxidatively generated
810 complex DNA damage: Tandem and clustered lesions. Cancer Lett. 2012;327: 5–15.
811 doi:https://doi.org/10.1016/j.canlet.2012.04.005
812 46. Chanet R, Heude M, Adjiri a, Maloisel L, Fabre F. Semidominant mutations in the
813 yeast Rad51 protein and their relationships with the Srs2 helicase. Mol Cell Biol.
814 1996;16: 4782–9. Available:

815 http://www.pubmedcentral.nih.gov/articlerender.fcgi?artid=231479&tool=pmcentrez&
816 rendertype=abstract
817 47. Game JC, Mortimer RK. A genetic study of X-ray sensitive mutants in yeast. Mutat
818 Res - Fundam Mol Mech Mutagen. 1974; doi:10.1016/0027-5107(74)90176-6
819 48. Lettier G, Feng Q, De Mayolo AA, Erdeniz N, Reid RJD, Lisby M, et al. The role of
820 DNA double-strand breaks in spontaneous homologous recombination in S. cerevisiae.
821 PLoS Genet. 2006;2: 1773–1786. doi:10.1371/journal.pgen.0020194
822 49. Coïc E, Gluck L, Fabre F. Evidence for short-patch mismatch repair in Saccharomyces
823 cerevisiae. EMBO J. 2000; doi:10.1093/emboj/19.13.3408
824 50. Petes T. 8 Recombination in Yeast. Cold Spring Harbor …. 1991.
825 51. Friis J, Roman H. The effect of the mating-type alleles on intragenic recombination in
826 yeast. Genetics. 1968;
827 52. Lisby M, Barlow JH, Burgess RC, Rothstein R. Choreography of the DNA damage
828 response: Spatiotemporal relationships among checkpoint and repair proteins. Cell.
829 2004;118: 699–713. doi:10.1016/j.cell.2004.08.015
830 53. Rossodivita AA, Boudoures AL, Mecoli JP, Steenkiste EM, Karl AL, Vines EM, et al.
831 Histone H3 K79 methylation states play distinct roles in UV-induced sister chromatid
832 exchange and cell cycle checkpoint arrest in Saccharomyces cerevisiae. Nucleic Acids
833 Res. 2014;42: 6286–6299. doi:10.1093/nar/gku242
834 54. Lemontt JF. Pathways of ultraviolet mutability in Saccharomyces cerevisiae. I. Some
835 properties of double mutants involving uvs9 and rev. Mutat Res - Fundam Mol Mech
836 Mutagen. 1971; doi:10.1016/0027-5107(71)90041-8
837 55. Lovett ST, Mortimer RK. Characterization of null mutants of the RAD55 gene of
838 Saccharomyces cerevisiae: effects of temperature, osmotic strength and mating type.
839 Genetics. 1987;

840 56. Heude M, Fabre F. a/α-control of DNA repair in the yeast Saccharomyces cerevisiae:
841 Genetic and physiological aspects. Genetics. 1993;
842 57. Valencia-Burton M, Oki M, Johnson J, Seier TA, Kamakaka R, Haber JE. Different
843 mating-type-regulated genes affect the DNA repair defects of saccharomyces RAD51,
844 RAD52 and RAD55 mutants. Genetics. 2006; doi:10.1534/genetics.106.058685
845 58. Quah SK, Von Borstel RC, Hastings PJ. The origin of spontaneous mutation in
846 Saccharomyces cerevisiae. Genetics. 1980; doi:10.1093/genetics/96.4.819
847 59. Tellier-Lebegue C, Dizet E, Ma E, Veaute X, Coïc E, Charbonnier J-B, et al. The
848 translesion DNA polymerases Pol ζ and Rev1 are activated independently of PCNA
849 ubiquitination upon UV radiation in mutants of DNA polymerase δ. PLoS Genet.
850 2017;13. doi:10.1371/journal.pgen.1007119
851 60. Whelan WL, Gocke E, Manney TR. The CAN1 locus of Saccharomyces cerevisiae:
852 Fine-structure analysis and forward mutation rates. Genetics. 1979;
853 doi:10.1093/genetics/91.1.35
854 61. Aboussekhra A, Chanet R, Zgaga Z, Cassier-Chauvat C, Heude M, Fabre F. RADH, a
855 gene of Saccharomyces cerevisiae encoding a putative DNA helicase involved in DNA
856 repair. Characteristics of radH mutants and sequence of the gene. Nucleic Acids Res.
857 1989; doi:10.1093/nar/17.18.7211
858 62. Gangloff S, Soustelle C, Fabre F. Homologous recombination is responsible for cell
859 death in the absence of the Sgs1 and Srs2 helicases. Nat Genet. 2000;25: 192–194.
860 doi:10.1038/76055
861 63. Klein HL. Mutations in recombinational repair and in checkpoint control genes
862 suppress the lethal combination of srs2Δ with other DNA repair genes in
863 Saccharomycescerevisiae. Genetics. 2001;157: 557–565.
864 64. Fabre F, Chan A, Heyer WD, Gangloff S. Alternate pathways involving Sgs1/Top3,

865 Mus81/ Mms4, and Srs2 prevent formation of toxic recombination intermediates from
866 single-stranded gaps created by DNA replication. Proc Natl Acad Sci U S A. 2002;99:
867 16887–16892. doi:10.1073/pnas.252652399
868 65. Rong L, Palladino F, Aguilera A, Klein HL. The hyper-gene conversion hpr5-1
869 mutation of Saccharomyces cerevisiae is an allele of the SRS2/RADH gene. Genetics.
870 1991;127: 75 LP – 85. Available: http://www.genetics.org/content/127/1/75.abstract
871 66. Esta A, Ma E, Dupaigne P, Maloisel L, Guerois R, Le Cam E, et al. Rad52 sumoylation
872 prevents the toxicity of unproductive Rad51 filaments independently of the anti-
873 recombinase Srs2. PLoS Genet. 2013;9: e1003833. doi:10.1371/journal.pgen.1003833
874 67. Ira G, Malkova A, Liberi G, Foiani M, Haber JE. Srs2 and Sgs1-Top3 suppress
875 crossovers during double-strand break repair in yeast. Cell. 2003;115: 401–11.
876 Available:
877 http://www.ncbi.nlm.nih.gov/pubmed/14622595%0Ahttp://www.pubmedcentral.nih.go
878 v/articlerender.fcgi?artid=PMC4493758
879 68. Urulangodi M, Sebesta M, Menolfi D, Szakal B, Sollier J, Sisakova A, et al. Local
880 regulation of the Srs2 helicase by the SUMO-like domain protein Esc2 promotes
881 recombination at sites of stalled replication. Genes Dev. 2015;29: 2067–2080.
882 doi:10.1101/gad.265629.115
883 69. Arbel M, Bronstein A, Sau S, Liefshitz B, Kupiec M. Access to pcna by srs2 and elg1
884 controls the choice between alternative repair pathways in saccharomyces cerevisiae.
885 MBio. 2020;11: 1–14. doi:10.1128/mBio.00705-20
886 70. Panzarino NJ, Krais JJ, Cong K, Peng M, Mosqueda M, Nayak SU, et al. Replication
887 Gaps Underlie BRCA Deficiency and Therapy Response. Cancer Res. 2021;81: 1388–
888 1397. doi:10.1158/0008-5472.CAN-20-1602
889 71. Cong K, Peng M, Kousholt AN, Lee WTC, Lee S, Nayak S, et al. Replication gaps are

890 a key determinant of PARP inhibitor synthetic lethality with BRCA deficiency. Mol
891 Cell. 2021;81: 3128-3144.e7. doi:https://doi.org/10.1016/j.molcel.2021.06.011
892 72. Piberger AL, Bowry A, Kelly RDW, Walker AK, González-Acosta D, Bailey LJ, et al.
893 PrimPol-dependent single-stranded gap formation mediates homologous recombination
894 at bulky DNA adducts. Nat Commun. 2020; doi:10.1038/s41467-020-19570-7
895 73. Alexandrov LB, Nik-Zainal S, Wedge DC, Aparicio SAJR, Behjati S, Biankin A V., et
896 al. Signatures of mutational processes in human cancer. Nature. 2013;500: 415–421.
897 doi:10.1038/nature12477
898 74. Nik-Zainal S, Davies H, Staaf J, Ramakrishna M, Glodzik D, Zou X, et al. Landscape
899 of somatic mutations in 560 breast cancer whole-genome sequences. Nature. 2016;534:
900 47–54. doi:10.1038/nature17676
901 75. Nolan E, Savas P, Policheni AN, Darcy PK, Vaillant F, Mintoff CP, et al. Combined
902 immune checkpoint blockade as a therapeutic strategy for BRCA1-mutated breast
903 cancer. Sci Transl Med. 2017;9. doi:10.1126/scitranslmed.aal4922
904 76. Wen WX, Leong CO. Association of BRCA1- And BRCA2-deficiency with mutation
905 burden, expression of PD-L1/ PD-1, immune infiltrates, and T cell-inflamed signature
906 in breast cancer. PLoS One. 2019;14: 1–16. doi:10.1371/journal.pone.0215381
907 77. Taglialatela A, Leuzzi G, Sannino V, Cuella-Martin R, Huang J-W, Wu-Baer F, et al.
908 REV1-Polζ maintains the viability of homologous recombination-deficient cancer cells
909 through mutagenic repair of PRIMPOL-dependent ssDNA gaps. Mol Cell. 2021;81:
910 4008-4025.e7. doi:https://doi.org/10.1016/j.molcel.2021.08.016
911 78. Hurley D. In the Clinic. Neurol Today. 2017;17: 22–23.
912 doi:10.1097/01.nt.0000521902.81399.b2
913 79. Zhou J, Gelot C, Pantelidou C, Li A, Yücel H, Davis RE, et al. A first-in-class
914 polymerase theta inhibitor selectively targets homologous-recombination-deficient

915 tumors. Nat Cancer. 2021;2: 598–610. doi:10.1038/s43018-021-00203-x

916 80. Zatreanu D, Robinson HMR, Alkhatib O, Boursier M, Finch H, Geo L, et al. Polθ
917 inhibitors elicit BRCA-gene synthetic lethality and target PARP inhibitor resistance.
918 Nat Commun. 2021;12: 3636. doi:10.1038/s41467-021-23463-8

919 81. Wojtaszek JL, Chatterjee N, Najeeb J, Ramos A, Lee M, Bian K, et al. A Small
920 Molecule Targeting Mutagenic Translesion Synthesis Improves Chemotherapy. Cell.
921 2019;178: 152-159.e11. doi:10.1016/j.cell.2019.05.028

922 82. Baudin a, Ozier-Kalogeropoulos O, Denouel a, Lacroute F, Cullin C. A simple and
923 efficient method for direct gene deletion in Saccharomyces cerevisiae. Nucleic Acids
924 Res. 1993;21: 3329–3330. doi:10.1093/nar/21.14.3329

925 83. Longtine MS, McKenzie A, Demarini DJ, Shah NG, Wach A, Brachat A, et al.
926 Additional modules for versatile and economical PCR-based gene deletion and
927 modification in Saccharomyces cerevisiae. Yeast. 1998;14: 953–61.
928 doi:10.1002/(SICI)1097-0061(199807)14:10<953::AID-YEA293>3.0.CO;2-U

929 84. Sherman F. Getting started with yeast. Methods Enzymol. 2002;350: 3–41.
930 doi:10.1016/S0076-6879(02)50954-X

931 85. Ma CM, Coffey CW, DeWerd LA, Liu C, Nath R, Seltzer SM, et al. AAPM protocol
932 for 40-300 kV x-ray beam dosimetry in radiotherapy and radiobiology. Med Phys.
933 2001;28: 868–893. doi:10.1118/1.1374247

934 86. Spell RM, Jinks-Robertson S. Determination of mitotic recombination rates by
935 fluctuation analysis in Saccharomyces cerevisiae. Methods Mol Biol. 2004;

936

937
938

Figure 1

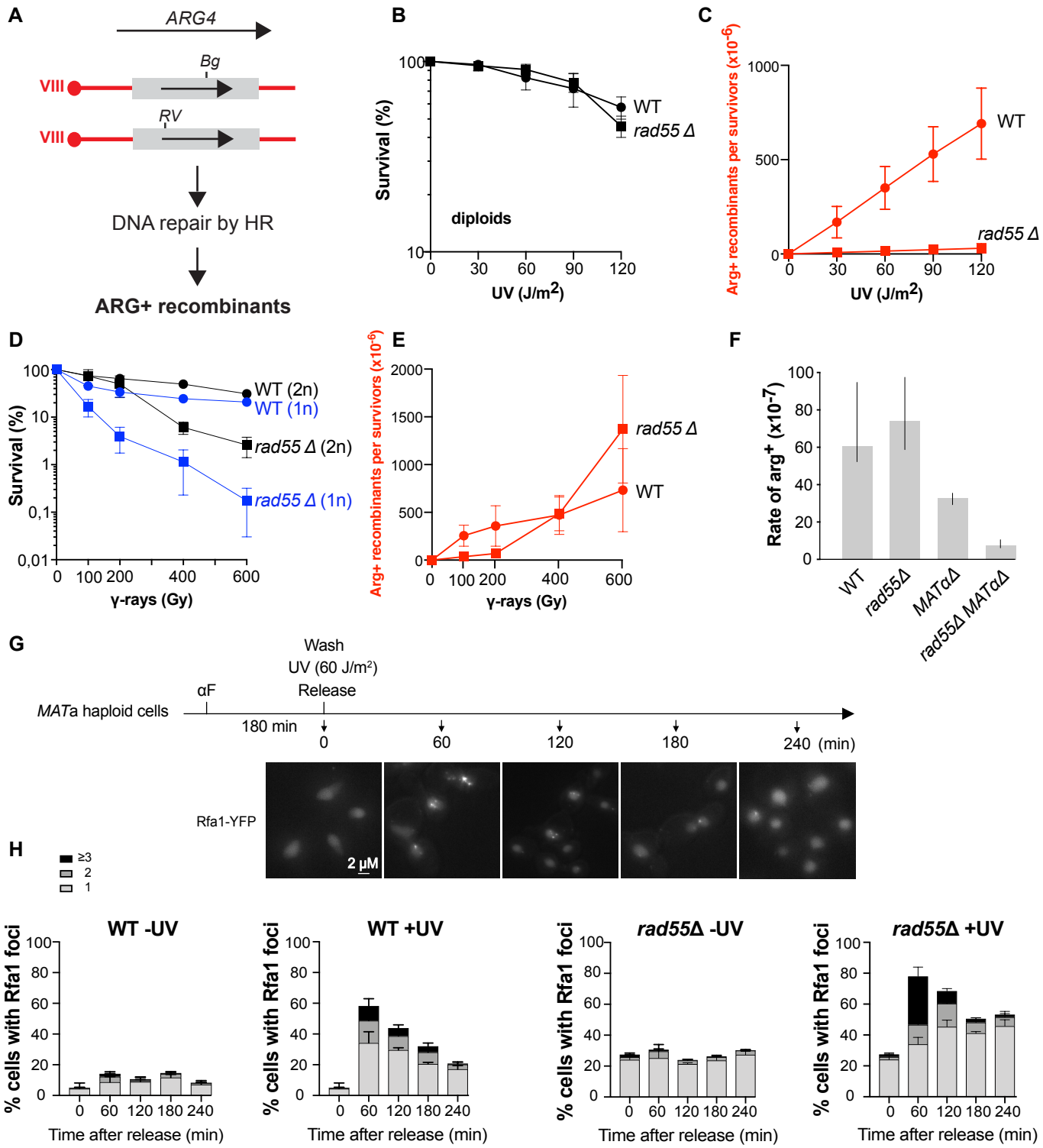
A
ARG4
Bg
VIII
RV
VIII
DNA repair by HR
ARG+ recombinants
B
Survival (%)
diploids
WT
rad55 Δ
UV (J/m2)
C
Arg+ recombinants per survivors (x10-6)
WT
rad55 Δ
UV (J/m2)
D
Survival (%)
WT (2n)
WT (1n)
rad55 Δ (2n)
rad55 Δ (1n)
γ-rays (Gy)
E
Arg+ recombinants per survivors (x10-6)
rad55 Δ
WT
γ-rays (Gy)
F
Rate of arg+ (x10-7)
WT
rad55Δ
MATαΔ
rad55Δ MATαΔ
G
Wash
UV (60 J/m2)
αF
Release
MATa haploid cells
180 min
0
60
120
180
240 (min)
Rfa1-YFP
2 μM
H
≥3
2
1
WT -UV
WT +UV
rad55Δ -UV
rad55Δ +UV
% cells with Rfa1 foci
Time after release (min)

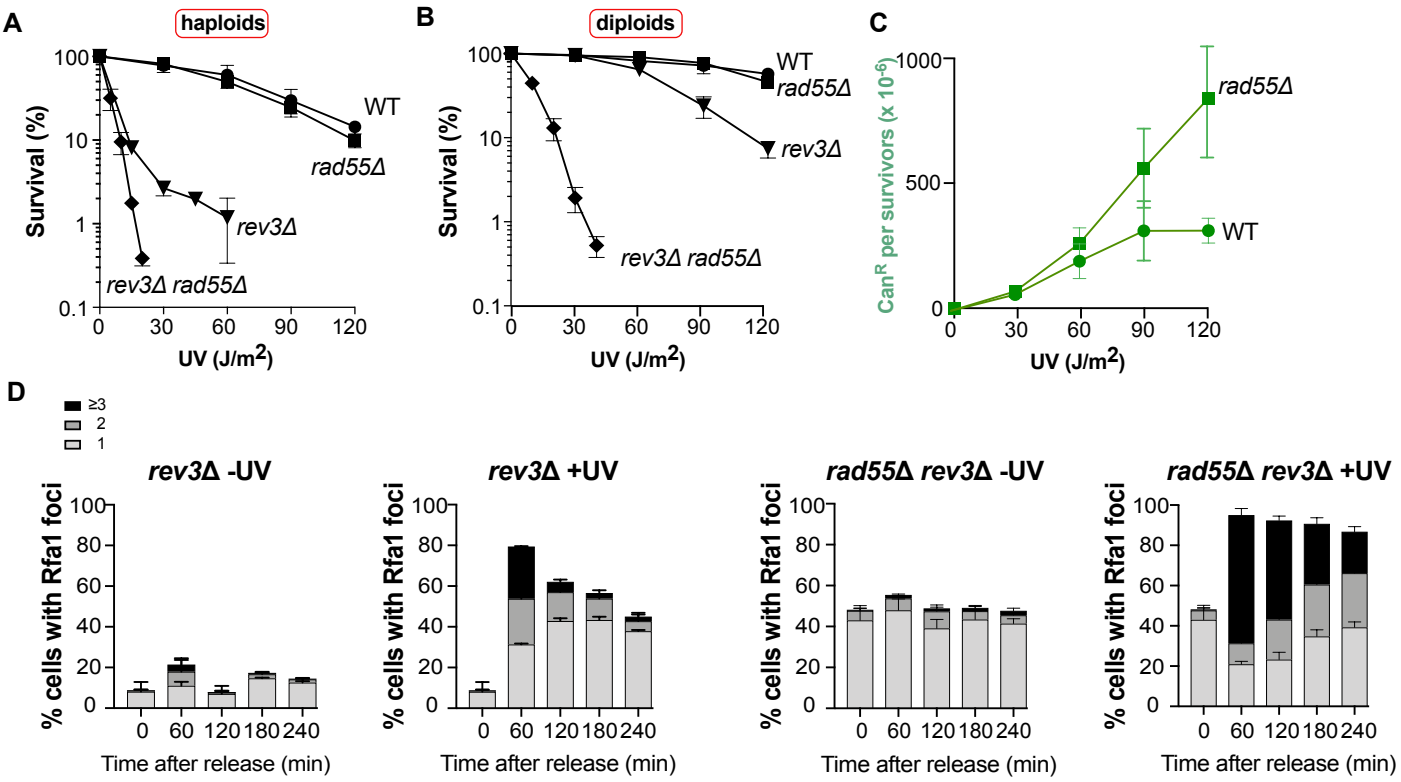
A
haploids
Survival (%)
UV (J/m2)
WT
rad55Δ
rev3Δ
rev3Δ rad55Δ
B
diploids
Survival (%)
UV (J/m2)
WT
rad55Δ
rev3Δ
rev3Δ rad55Δ
C
CanR per survivors (x 10-6)
UV (J/m2)
rad55Δ
WT
D
≥3
2
1
rev3Δ -UV
rev3Δ +UV
rad55Δ rev3Δ -UV
rad55Δ rev3Δ +UV
% cells with Rfa1 foci
Time after release (min)

Figure 2

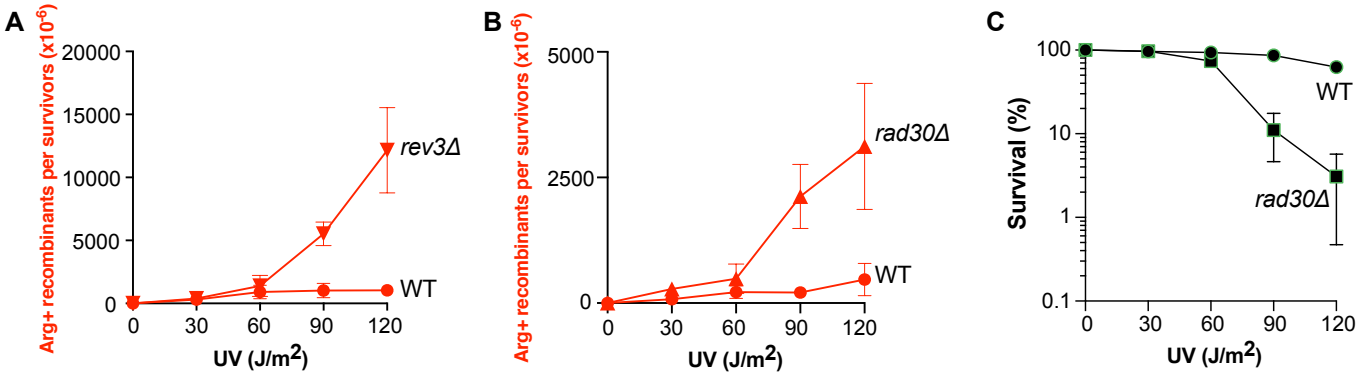
A
Arg+ recombinants per survivors (x10-6)
20000
15000
10000
5000
0
rev3Δ
WT
0
30
60
90
120
UV (J/m2)
B
Arg+ recombinants per survivors (x10-6)
5000
2500
0
rad30Δ
WT
0
30
60
90
120
UV (J/m2)
C
Survival (%)
100
10
1
0.1
WT
rad30Δ
0
30
60
90
120
UV (J/m2)

Figure 3

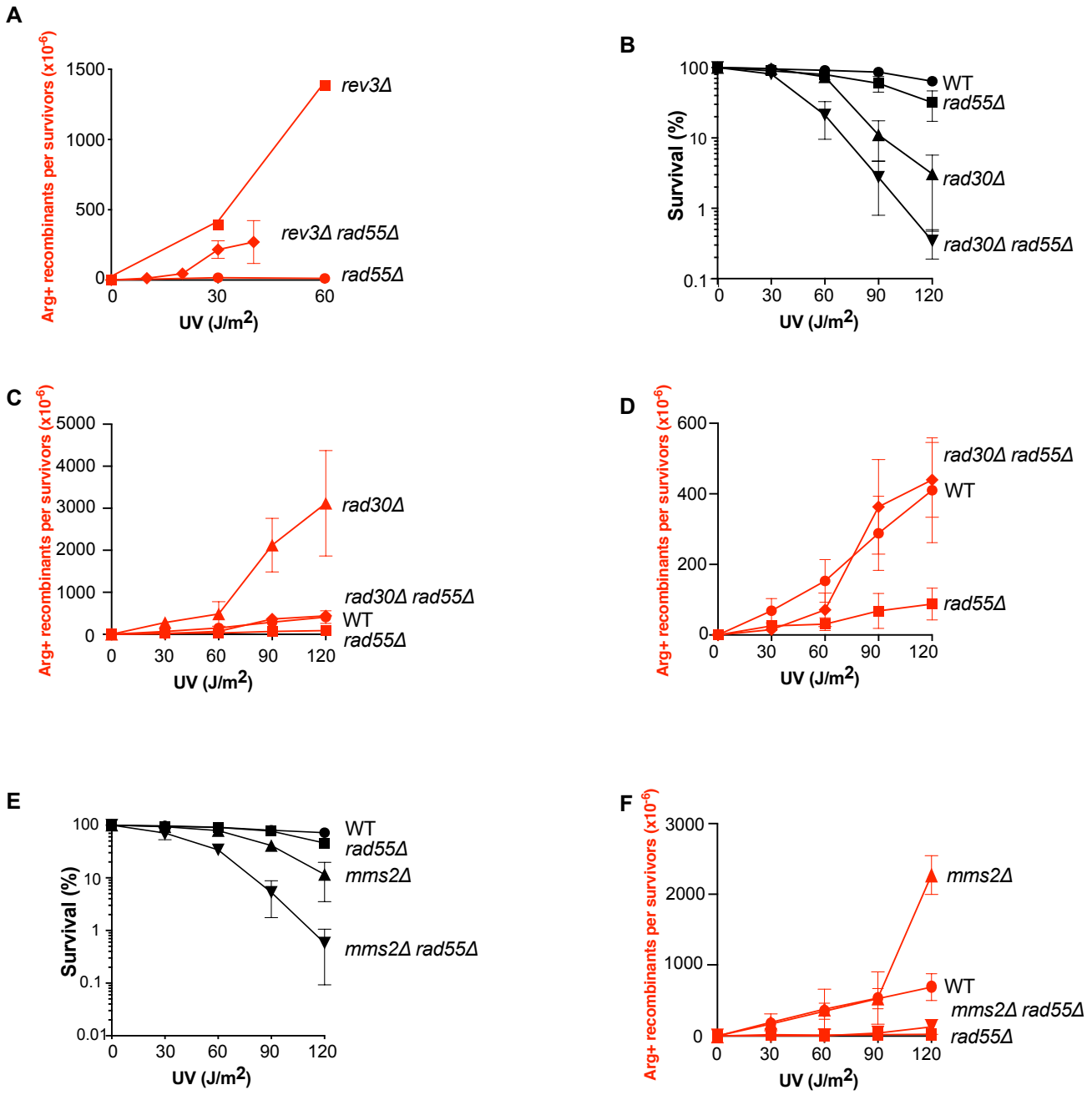
A
Arg+ recombinants per survivors (x10-6)
1500
1000
500
0
0
30
60
UV (J/m2)
rev3Δ
rev3Δ rad55Δ
rad55Δ
B
Survival (%)
100
10
1
0.1
0
30
60
90
120
UV (J/m2)
WT
rad55Δ
rad30Δ
rad30Δ rad55Δ
C
Arg+ recombinants per survivors (x10-6)
5000
4000
3000
2000
1000
0
0
30
60
90
120
UV (J/m2)
rad30Δ
rad30Δ rad55Δ
WT
rad55Δ
D
Arg+ recombinants per survivors (x10-6)
600
400
200
0
0
30
60
90
120
UV (J/m2)
rad30Δ rad55Δ
WT
rad55Δ
E
Survival (%)
100
10
1
0.1
0.01
0
30
60
90
120
UV (J/m2)
WT
rad55Δ
mms2Δ
mms2Δ rad55Δ
F
Arg+ recombinants per survivors (x10-6)
3000
2000
1000
0
0
30
60
90
120
UV (J/m2)
mms2Δ
WT
mms2Δ rad55Δ
rad55Δ

Figure 4

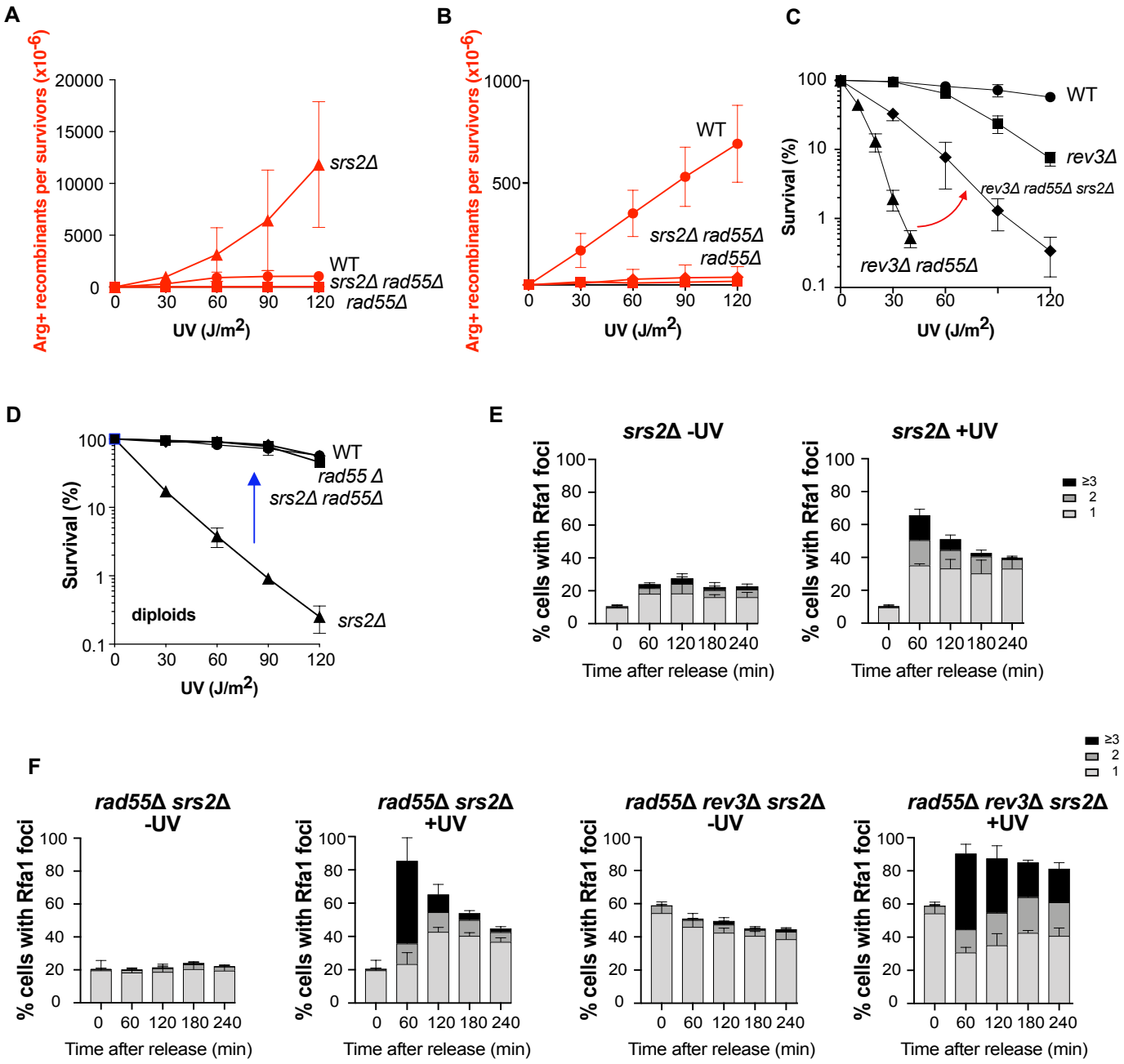
A
Arg+ recombinants per survivors (x10^-6)
20000
15000
10000
5000
0
srs2Δ
WT
srs2Δ rad55Δ
rad55Δ
0 30 60 90 120
UV (J/m2)
B
Arg+ recombinants per survivors (x10^-6)
1000
500
WT
srs2Δ rad55Δ
rad55Δ
0 30 60 90 120
UV (J/m2)
C
Survival (%)
100
10
1
0.1
WT
rev3Δ
rev3Δ rad55Δ srs2Δ
rev3Δ rad55Δ
0 30 60 120
UV (J/m2)
D
Survival (%)
100
10
1
0.1
WT
rad55 Δ
srs2Δ rad55Δ
diploids
srs2Δ
0 30 60 90 120
UV (J/m2)
E
srs2Δ -UV
srs2Δ +UV
% cells with Rfa1 foci
100
80
60
40
20
0
≥3
2
1
0 60 120 180 240
Time after release (min)
F
rad55Δ srs2Δ -UV
rad55Δ srs2Δ +UV
rad55Δ rev3Δ srs2Δ -UV
rad55Δ rev3Δ srs2Δ +UV
% cells with Rfa1 foci
Time after release (min)

Figure 5

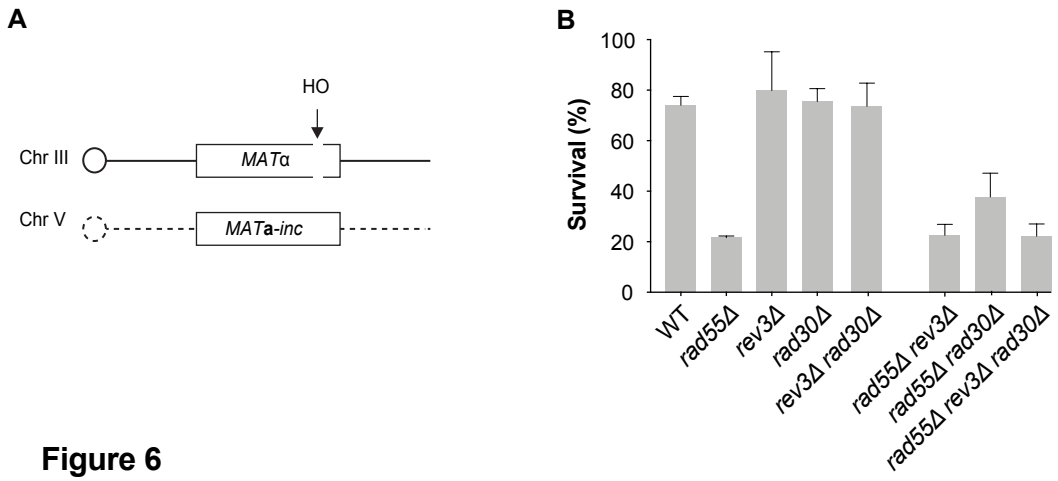
A
HO
Chr III
MATα
Chr V
MATa-inc
B
Survival (%)
100
80
60
40
20
0
WT
rad55Δ
rev3Δ
rad30Δ
rev3Δ rad30Δ
rad55Δ rev3Δ
rad55Δ rad30Δ
rad55Δ rev3Δ rad30Δ

Figure 6

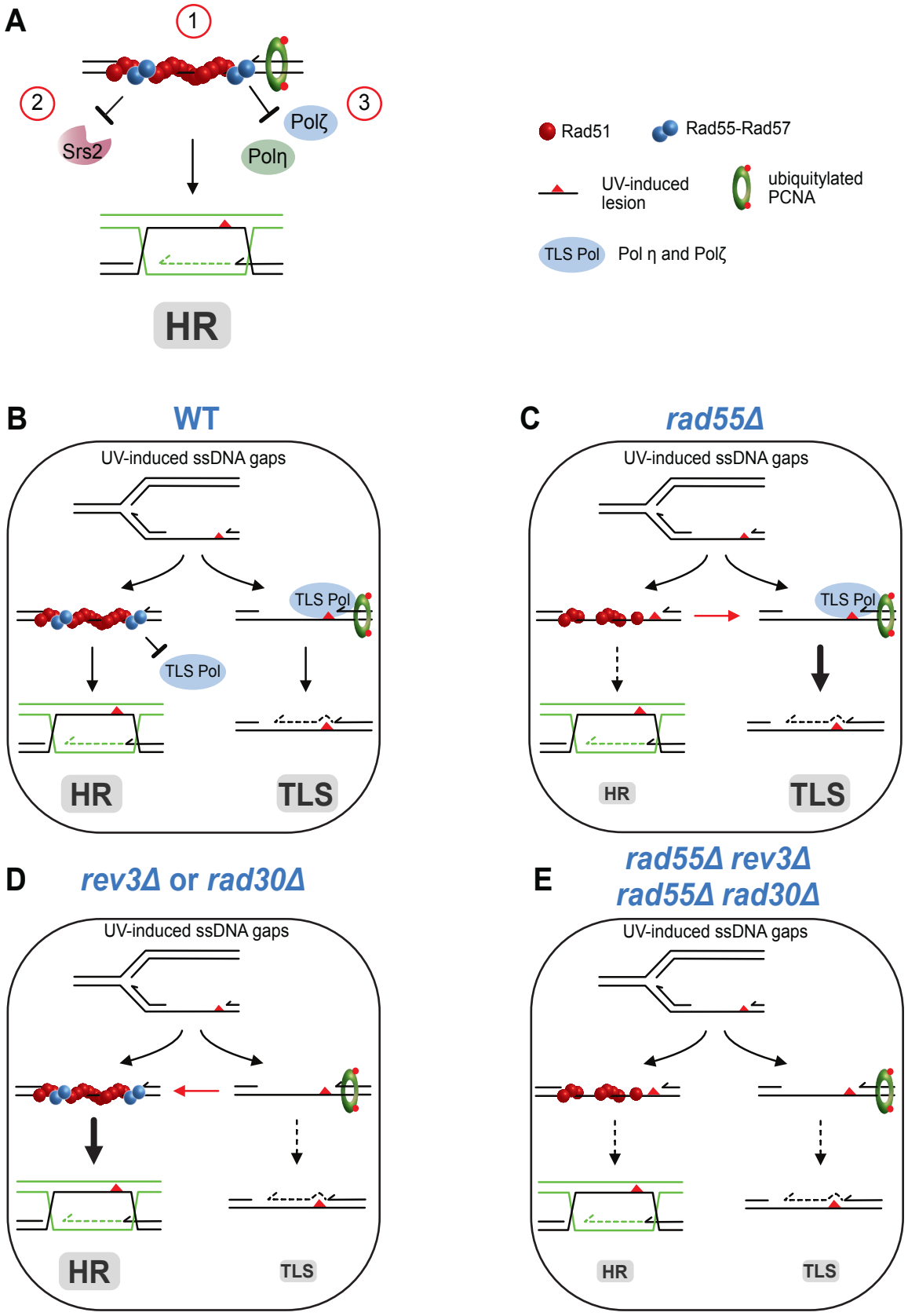
A
1
2
3
Srs2
Polζ
Polη
HR
Rad51
Rad55-Rad57
UV-induced lesion
ubiquitylated PCNA
TLS Pol
Pol η and Polζ
B
WT
UV-induced ssDNA gaps
TLS Pol
TLS Pol
HR
TLS
C
rad55Δ
UV-induced ssDNA gaps
TLS Pol
HR
TLS
D
rev3Δ or rad30Δ
UV-induced ssDNA gaps
HR
TLS
E
rad55Δ rev3Δ
rad55Δ rad30Δ
UV-induced ssDNA gaps
HR
TLS

Figure 7

Supplemental Figure S1

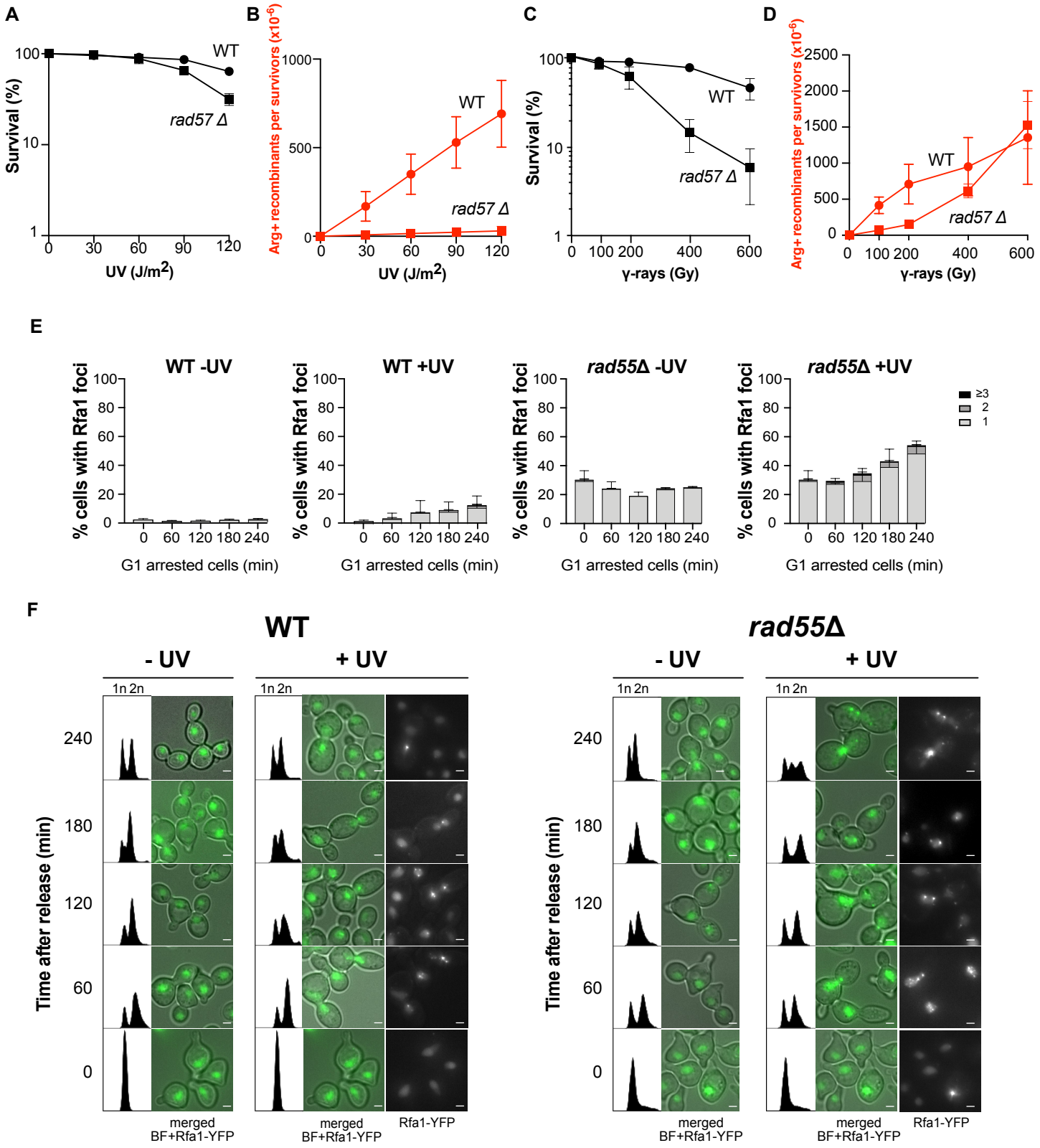

Supplemental Figure S2

A

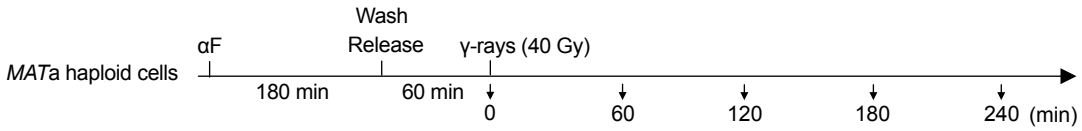

B

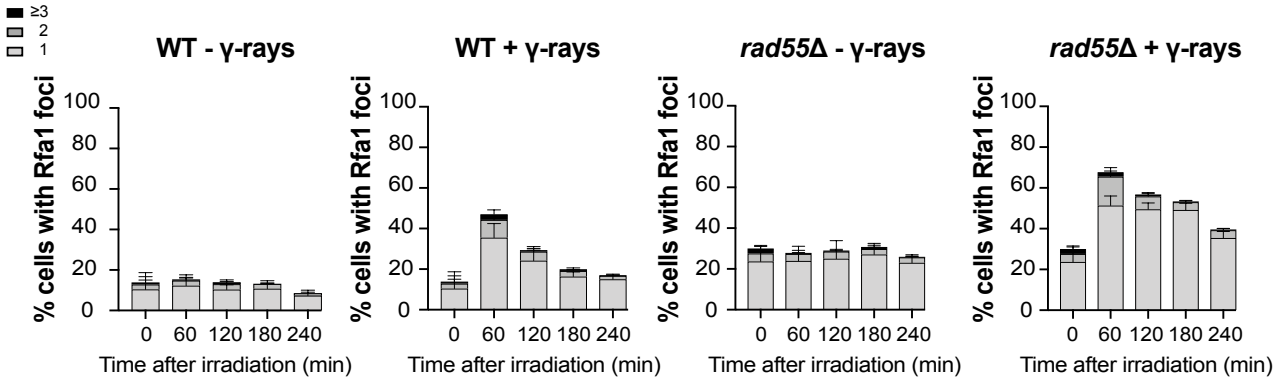

Supplemental Figure S3

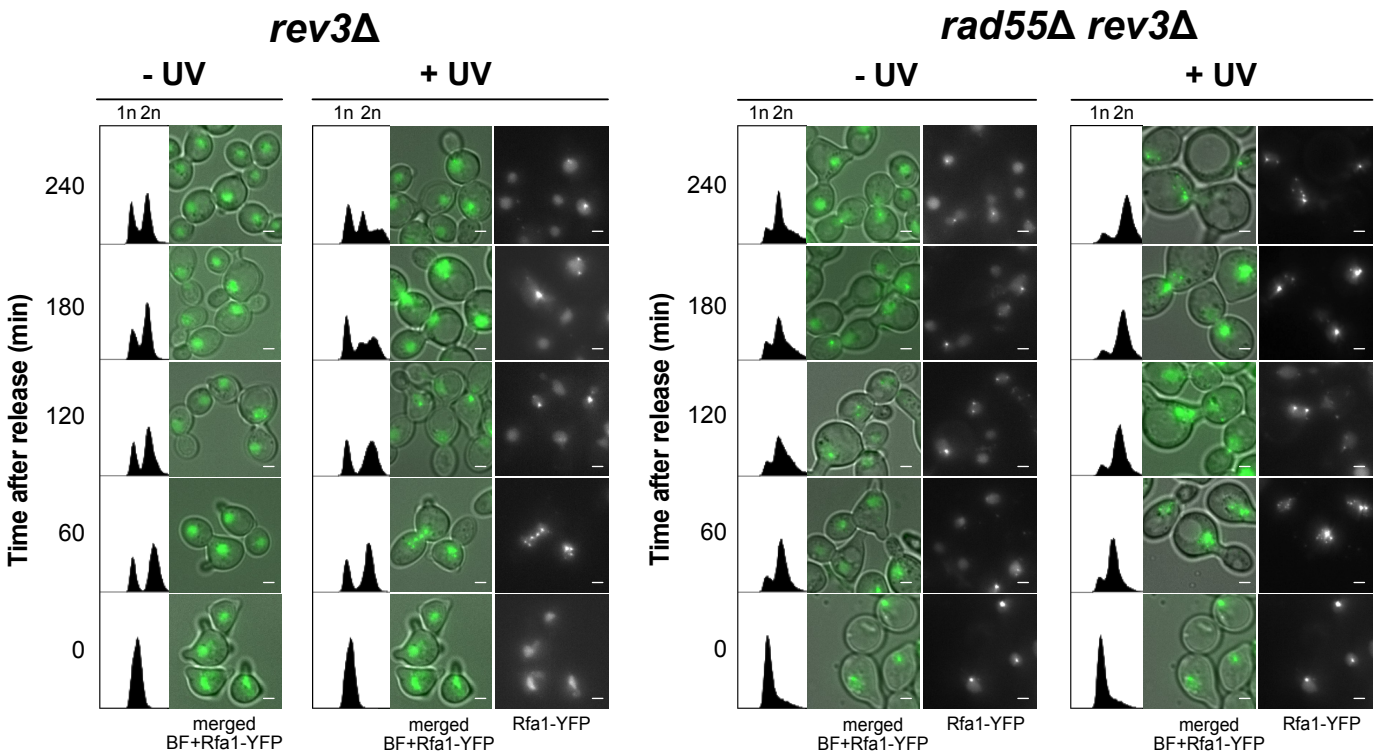

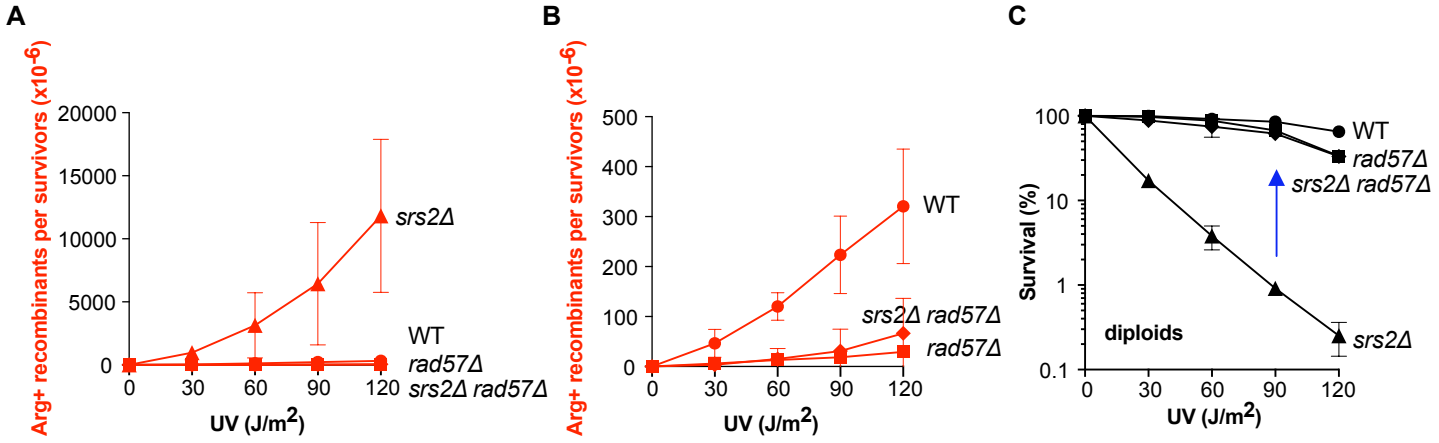

Supplemental Figure S4
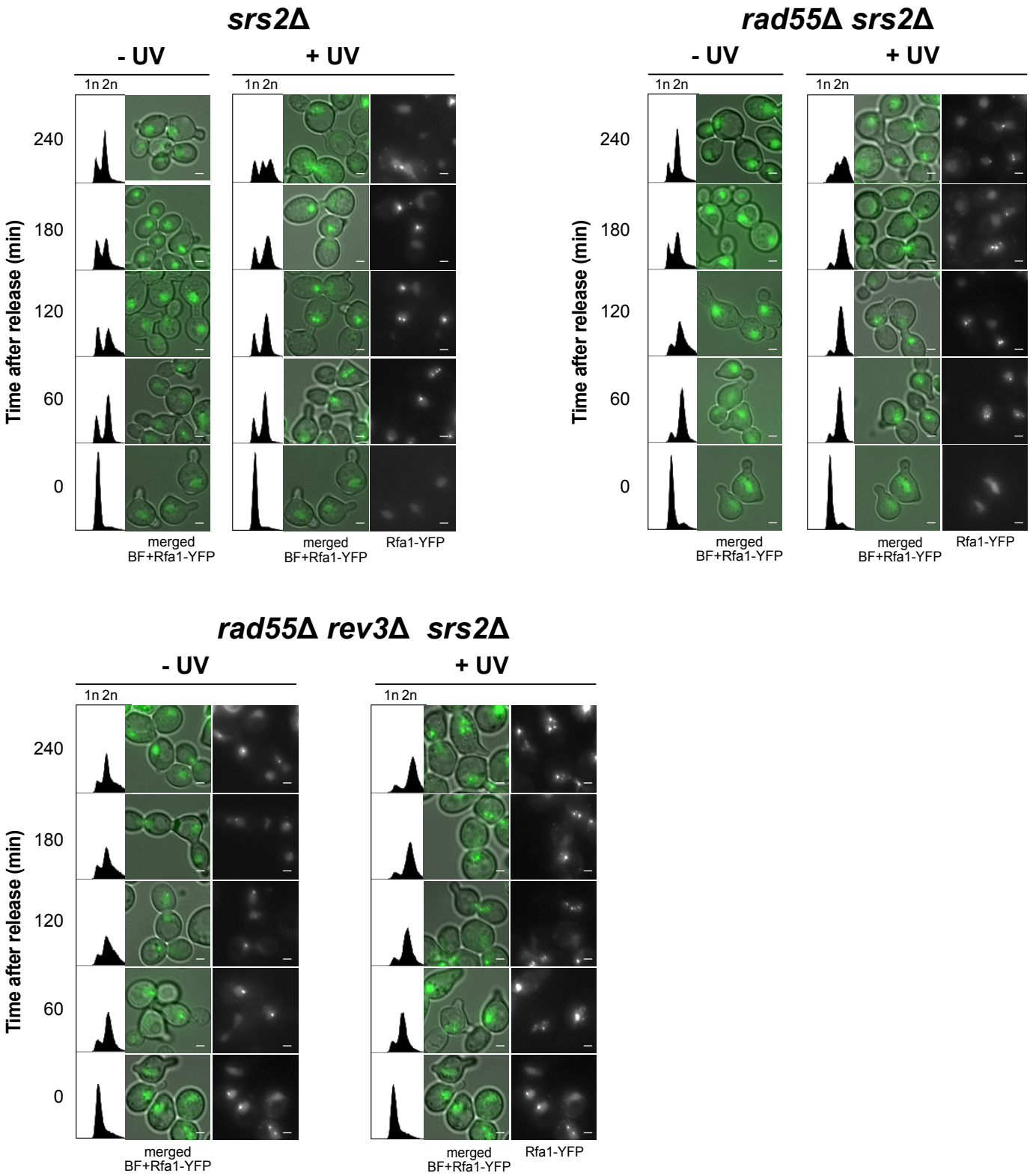
Supplemental Figure S5